Received: 3 July 2021 | Revised: 25 November 2021 | Accepted: 29 December 2021

DOI: 10.1002/jev2.12185

RESEARCH ARTICLE

Extracellular vesicle-mediated delivery of circDYM alleviates CUS-induced depressive-like behaviours

Xiaoyu Yu[1] | **Ying Bai**[1] | **Bing Han**[1] | **Minzi Ju**[1] | **Tianci Tang**[1] | **Ling Shen**[1] | **Mingyue Li**[1] | **Li Yang**[1] | **Zhao Zhang**[2] | **Guoku Hu**[3] | **Jie Chao**[4] | **Yuan Zhang**[1] | **Honghong Yao**[1,5,6,7]

[1] Department of Pharmacology, School of Medicine, Southeast University, Nanjing, Jiangsu, China

[2] State Key Laboratory of Bioactive Substances and Functions of Natural Medicines, Institute of Materia Medica & Neuroscience Center, Chinese Academy of Medical Sciences and Peking Union Medical College, Beijing, China

[3] Department of Pharmacology and Experimental Neuroscience, University of Nebraska Medical Center, Omaha, Nebraska, USA

[4] Department of Physiology, School of Medicine, Southeast University, Nanjing, Jiangsu, China

[5] Jiangsu Provincial Key Laboratory of Critical Care Medicine, Southeast University, Nanjing, Jiangsu, China

[6] Co-innovation Center of Neuroregeneration, Nantong University, Nantong, Jiangsu, China

[7] Institute of Life Sciences, Key Laboratory of Developmental Genes and Human Disease, Southeast University, Nanjing, Jiangsu, China

Correspondence
Honghong Yao, PhD, and Yuan Zhang, PhD, Department of Pharmacology, Medical School of Southeast University, Nanjing 210009, Jiangsu, China.
Email: yaohh@seu.edu.cn and yuanzhang@seu.edu.cn

Funding information
National Natural Science Foundation of Distinguished Young Scholars, Grant/Award Number: 82025033; National Key Research and Development Program of China, Grant/Award Numbers: 2021ZD0202900, 2017YFA0104303; National Natural Science Foundation of China, Grant/Award Numbers: 81761138048, 81673410, 81973304; CAMS Innovation Fund for Medical Sciences (CIFMS), Grant/Award Number: 2016-I2M-1-004; Natural Science Foundation of Jiangsu Province, Grant/Award Number: BK20191265; National Science and Technology Major Project, Grant/Award Number: 2020 ZX09201015; Fundamental Research Funds for the Central Universities, Grant/Award Number: 2242021R41098; Jiangsu Innovation and Entrepreneurship Team Program

Abstract

Major depressive disorder (MDD) is the most prevalent psychiatric disorder worldwide and severely limits psychosocial function and quality of life, but no effective medication is currently available. Circular RNAs (circRNAs) have been revealed to participate in the MDD pathological process. Targeted delivery of circRNAs without blood-brain barrier (BBB) restriction for remission of MDD represents a promising approach for antidepressant therapy. In this study, RVG-circDYM-extracellular vesicles (RVG-circDYM-EVs) were engineered to target and preferentially transfer circDYM to the brain, and the effect on the pathological process in a chronic unpredictable stress (CUS) mouse model of depression was investigated. The results showed that RVG-circDYM-EVs were successfully purified by ultracentrifugation from overexpressed circDYM HEK 293T cells, and the characterization of RVG-circDYM-EVs was successfully demonstrated in terms of size, morphology and specific markers. Beyond demonstrating proof-of-concept for an RNA drug delivery technology, we observed that systemic administration of RVG-circDYM-EVs efficiently delivered circDYM to the brain, and alleviated CUS-induced depressive-like behaviours, and we discovered that RVG-circDYM-EVs notably inhibited microglial activation, BBB leakiness and peripheral immune cells infiltration, and attenuated astrocyte disfunction induced by CUS. CircDYM can bind mechanistically to the transcription factor TAF1 (TATA-box binding protein associated factor 1), resulting in the decreased expression of its downstream target genes with consequently suppressed neuroinflammation. Taken together, our findings suggest that extracellular vesicle-mediated delivery of circDYM is effective for MDD treatment and promising for clinical applications.

KEYWORDS
CircDYM, extracellular vesicles, inflammation, MDD, TAF1

1 | INTRODUCTION

Major depressive disorder (MDD) is a chronic disease that severely impairs psychosocial function and reduces quality of life, and is the second leading cause of disability globally, with an estimated 350 million people worldwide expected to suffer from MDD by 2030 (Charlson et al., 2019; Malhi & Mann, 2018; Saxena et al., 2013; Smith, 2014). The pathogenesis of MDD is complex and can be both congenital and acquired; its common clinical manifestations include obvious and persistent depression, anhedonia, pessimism, and suicidal tendency (Arnow et al., 2015; Wray et al., 2018). Although current treatments for MDD include a variety of chemicals, peptides, and gene therapy, nearly a third of patients with MDD are insensitive to existing drugs (Belzeaux et al., 2020; Davey et al., 2019; Meltzer-Brody et al., 2018; Murrough et al., 2017). Moreover, the blood-brain barrier (BBB) greatly limits most drugs from accessing the brain, leading to unsatisfactory therapeutic outcomes for MDD (El-Hage et al., 2013). Hence, more effective therapeutics without BBB restriction is critically needed.

Extracellular vesicles (EVs) are lipid bilayer membrane-enclosed nanoscale particles released from various cell types. They can be classified based on physical characteristics into small EVs and medium/large EVs according to the International Society for Extracellular Vesicles (ISEV) (Théry et al., 2018). The released EVs function as intercellular messengers by transferring proteins and nucleotides to neighbouring or distant cells (Wiklander et al., 2019). Due to their low immunogenicity, biodegradability, low toxicity, strong ability to protect endogenous biologically active ingredients, and ability to pass through the BBB, EVs have become a new therapeutic method in the fields of immunotherapy, regenerative medicine, and drug delivery (Lener et al., 2015; Song et al., 2019). However, natural EVs lack targeting ability and accumulate rapidly in peripheral organs such as the liver and spleen after systemic administration, rather than targeting specific tissues (Wiklander et al., 2015). In recent years, studies have shown that specific ligands can be expressed on the membrane surface of EVs through gene modification, enabling targeted delivery of EVs (Kojima et al., 2018; Tian et al., 2014). For example, Alvarez-Erviti et al. (2011) modified EVs of dendritic cells with acetylcholine receptor (AChR)-specific rabies virus glycoprotein (RVG) peptides, thereby enabling the EVs to carry drugs effectively across the BBB for the treatment of brain diseases (Alvarez-Erviti et al., 2011).

Circular RNAs (circRNAs) are a class of non-coding RNAs with a closed continuous ring structure that are widely expressed in mammalian tissues (Kristensen et al., 2019). Mounting evidence suggests that circRNAs exhibit dynamic expression patterns under a series of physiological and pathological conditions, and play an important role in regulating protein expression, DNA methylation modification, and polypeptides translation (Chen et al., 2019; Liu et al., 2019; Yang et al., 2017). The participation of circRNAs in the pathogenesis of MDD attracted considerable attention because transcriptome analyses showed aberrant expression of circRNA in the peripheral blood of human and animal models with depression (Cui et al., 2016; Shi et al., 2021; Trautner et al., 1988). Our previous findings and others indicated that circRNAs could be a novel therapeutic target for improving depressive-like symptoms in various animal models (Huang et al., 2020; Zhang et al., 2018, 2019). CircDYM (mm9_circ_0007509), a homologous human and mouse circRNA, is derived from exons 4, 5 and 6 of the *DYM* gene. Other and our previous studies have indicated that the expression of circDYM was significantly reduced in plasma of patients with MDD as well as the plasma and hippocampus of depressive-like model mice (Song et al., 2020; Zhang et al., 2020).

Epidemiological studies have indicated that chronic exposure to stressful life events in the human population is considered a major risk factor for developing depression (Firk & Markus, 2007; Kendler et al., 2004). Chronic unpredictable stress (CUS) is established as a murine model that mimics the role of stress in the aetiology of depressive disorders in the human milieu. For context, the CUS model was developed by Latz in the 1980s and was subsequently improved by Willner et al., and to our understanding this is a widely employed model for rodent-based work in the depression research field (Katz & Sibel, 1982; Willner, 1984; Wohleb et al., 2018). Our previous studies and others applied CUS paradigm, in which experimental animals are housed in an inhospitable environment, where they are continuously exposed to a variety of unpredictable stimuli (e.g., light, social isolation, deprivation of food or water, etc.). The mice consistently exhibit depressive-like behaviours in this setting such as anhedonia and despair, thus mirroring the symptoms of MDD. Based on this CUS model, our findings demonstrated that overexpressed circDYM lentivirus microinjection in hippocampus of mice ameliorates depressive-like behaviours by targeting miR-9 to regulate microglial activation via HSP90 ubiquitination, indicating that circDYM may be a promising target for therapeutic interventions in MDD (Zhang et al., 2020). Although lentivirus-based gene therapy has been effective in basic medical experimental research, this method presents serious safety concerns in experimental clinical trials (Hacein-Bey-Abina et al., 2003, 2008).

The current study is based on the hypothesis that engineered EVs bearing circDYM can be delivered to the brain and exert therapeutic effects against CUS-induced depressive-like behaviours. Our results demonstrate that circDYM delivered by RVG-EVs can effectively alleviate depressive-like behaviours in mice by modulating neuroinflammation, thus illustrating an innovative strategy for the treatment of MDD.

2 | MATERIALS AND METHODS

2.1 | Cell culture

Primary mouse microglia were prepared from postnatal (P1 to P2) C57BL/6J mice, according to previous studies (Matcovitch-Natan et al., 2016; Zhang et al., 2020). Firstly, the membranes and blood vessels where disassociated and then the brain tissues were digested with trypsin-EDTA (25200056, Gibco) for 5 min. The supernatant was filtrated with a 70 μm nylon mesh and collected by centrifugation at 1200 rpm for 5 min. The cells were then seeded in 25 cm^2 cell culture flasks (430639, Corning), which were pre-coated with poly-D-lysine (P1024, Sigma-Aldrich). Cells were cultured with Dulbecco's modified Eagle's medium (DMEM, 10-013-CVR, Corning) supplemented with foetal bovine serum (FBS, 10% v/v, 10100147, Gibco) and penicillin-streptomycin (1% v/v, SV30010, Hyclone). The astrocytes reached confluence, and the cells began to grow in distinct layers after 7 days. Then, CSF2/GM-CSF (colony-stimulating factor [granulocyte-macrophage], 0.25 ng/ml) was added to the medium to aid microglial proliferation. Subsequently, the microglia were removed by shaking the flasks, and the supernatant was collected and centrifugated at 1500 rpm for 5 min. Finally, collected microglia were counted with a haematocytometer and seeded into a 24-well plate at a density of 2×10^5 per well. Moreover, microglia surface molecules, such as Iba-1, CD45 and CD11b were detected to identify primary mouse microglia in Figure S1.

The human embryonic kidney 293T cells (HEK 293T cells) were purchased from the Shanghai Cell Bank of Chinese Academy of Sciences (Shanghai, China), and cultured in DMEM supplemented with 10% FBS and 1% penicillin-streptomycin. In addition, FBS for EV production was depleted of bovine EVs by ultracentrifugation at 200,000 × *g* for 6 h at 4°C using an XPN-100 ultracentrifuge (Beckman Coulter, USA). The supernatant was then filtered through a 0.22-μm filter (Millipore, USA). All cells were kept in a humidified incubator (5% CO_2, 37°C).

2.2 | Transfection and preparation of EVs

HEK 293T cells were seeded in 225 cm^2 flasks (431082, Corning) and incubated at 37°C in 5% CO_2. When the cells reached approximately 70%–80% confluence, they were co-transfected with the vector or circDYM-GFP lentivirus (HANBIO, Shanghai, China) and RVG-Lamp2b plasmid (71294, ADDGENE) using Lipofectamine 2000 (11668019, Invitrogen) according to the manufacturer's instructions. Forty-eight h after transfection, hygromycin B (108435550, Roche) and puromycin (AK058, GPC Biotechnology) were added to the cell culture medium to obtain stable strains. RVG-EVs were prepared from the supernatant fluids of RVG-Vector-HEK 293T cells or RVG-circDYM-HEK 293T cells by differential centrifugation. Mock EVs (naïve EVs) were also prepared from HEK 293T cells without transfection of any lentiviruses or plasmids and used as controls. Briefly, the supernatant was centrifuged at 300 × *g* for 10 min, 3000 × *g* for 15 min, and 10,000 × *g* for 60 min at 4°C to remove cells and debris, and then filtered using a 0.22-μm filter (Millipore, USA). The filtrate was centrifuged at 200,000 × *g* for 90 min at 4°C using an XPN-100 ultracentrifuge (Beckman Coulter, USA). Subsequently, the pellet was resuspended in phosphate-buffered saline (PBS) and then ultracentrifuged again at 200,000 × *g* for 90 min. Finally, the resulting pellet was resuspended in PBS for further study.

2.3 | Collection of apoptotic bodies

The isolation process involves a three-step centrifugation. The initial centrifugation of the supernatant was at 300 × *g* for 10 min to remove cells. The supernatant was then subjected to a 3000 × *g* second centrifugation for 10 min to remove dead cells and debris. Finally, the remaining supernatant was subjected to a 10,000 × *g* ultracentrifugation for 60 min to obtain a pellet containing apoptotic bodies using an XPN-100 ultracentrifuge (Beckman Coulter, USA). The pellet was resuspended in PBS for further study.

2.4 | Characterization of EVs by western blotting

Well-established markers of purified EVs were verified by western blot analysis. The following antibodies were used: anti-CD63 (1:1000, 25682-1-AP, Proteintech group), anti-TSG101 (1:2000, 14497-1-AP, Proteintech group), anti-HA (1:3000, 51064-2-AP, Proteintech group), anti-Lamp2 (1:1000, 27823-1-AP, Proteintech group), anti-GM130 (1:5000, 66662-1-Ig, Proteintech group) and anti-Histone-H3 (1:1000, 17168-1-AP, Proteintech group).

2.5 | Examination of EVs by transmission electron microscopy (TEM)

The morphology of EVs was examined by TEM (H-7650C, HITACHI, Japan). In brief, ultra-concentrated EVs were fixed in 4% paraformaldehyde (PFA). Next, a drop of EV (10 μl) suspension was air-dried on formvar carbon-coated electron microscopy grid and then stained with 2% uranyl acetate (541-09-3, Chemical Book) for 5 min. Finally, the grids were observed under TEM operated at 80 kV.

2.6 | Quantification of EVs by nanoparticle tracking analysis (NTA)

NTA was used to visualize and quantitate nanoparticles in suspension. Briefly, as described previously (Elashiry et al., 2020), isolated EVs samples were appropriately diluted using PBS buffer. Next, the diluted EVs suspension (1 ml) was loaded into the sample chamber of ZetaView PMX 110 (Particle Metrix, Germany). Data analysis was performed with software (ZetaView 8.05.12). NTA measurement was recorded and analysed. The ZetaView system was calibrated using 100 polystyrene particles. The detailed size data of EVs were provided in Table S1.

2.7 | Concentration of EVs

Protein content in EVs was measured with a Pierce BCA Protein Assay Kit (P0011, Beyotime) following the manufacturer's protocol, which was used as an index of the amount of EVs. Samples of EVs (5 μl) were loaded into each well of a 96-well plate and 200 μl of BCA solution was added. The plate was incubated at 37°C for 30 min and the absorbance was detected at 562 nm using the Synergy H1 microplate reader (Biotek, USA). The final concentration of RVG-EVs was 1 mg protein ml^{-1} (about 1.2×10^{12} particles ml^{-1}). The proteins, RVG-EV counts and circDYM copy numbers as well as the ratio of circDYM/RVG-EVs are summarized in Table S2.

2.8 | Absolute quantitative polymerase chain reaction (qPCR)

Absolute qPCR was conducted to estimate the copy number of circDYM in overexpressed circDYM 293T cells and RVG-EVs. Briefly, a 177 bp characteristic segment containing the back-spliced junction of circDYM transcript was cloned and inserted into the pUC57 vector (Genscript, Nanjing). The different concentrations of plasmid by a factor of ten were used to plot a standard curve by real-time PCR. And the copy number of standard compounds according to the formula: copy number (copy/μl) = $6.02 \times 10^{23} \times$ plasmid concentration (ng/μl) $\times 10^{-9}$/[(molecular weight of vector + molecular weight of inserted fragment) $\times$ 660](g/mol). The amplification curve and the standard curve equation were obtained as: $Y = aX + b$ [log value on 10 of the initial amplification copy number was the abscissa (X), and the corresponding cycle number was the ordinate (Y)]. Cycle threshold (Ct) values of circDYM were calculated to arbitrary units using a linear equation of the plasmid standard allowing conclusions for the copy number of the circDYM.

2.9 | qPCR

RNA was extracted using TRIzol reagent (9109, TaKaRa) according to the manufacturer's protocol. First, genomic DNA was removed using template 200 ng RNA mixed with 2 μl 4 × gDNA wiper mix (R123-01, Vazyme) and nuclease free water up to 8 μl of the final reaction volume. This reaction mixture was incubated at 42°C for 2 min. Reverse transcription was then performed using the reaction tube mentioned above mixed with 2 μl of 5 × qRT SuperMix II (R123-01, Vazyme) and nuclease free water up to 10 μl of the final reaction volume. This reaction mixture was incubated at 50°C for 15 min and then for 2 min at 85°C. Next, the RT products (cDNA) obtained in the previous step were used as the template for qPCR. The qPCR reactions were carried out using SYBR Green qPCR Master Mix (Q141-02, Vazyme) containing 1 μl of cDNA in a 10 μl final volume reaction following the manufacturer's instructions in an Applied Biosystems qPCR System (StepOne, Thermo Fisher, USA) with the following cycling conditions: 5 min at 95°C followed by 30 cycles of 10 s at 95°C and 30 s at 60°C. The primers used to amplify circRNA and mRNA transcripts were synthesized by Invitrogen. The sequences of the primers are summarized in Table S3.

2.10 | RNA protection assay

RVG-circDYM-EVs (2.4×10^{12} particles) were incubated with 20 μl RNase A/T1 mix with or without 1% Triton X-100 at 37°C for 30 min. After inactivating at 75°C for 5 min, a total of 0.45 ml Trizol-LS was added immediately. RNA was extracted with miPure

Cell/Tissue miRNA kit (RC201, Vazyme), and then the same volume of RNA was reverse transcribed according to previous studies (Lin et al., 2020; Vu et al., 2019). Finally, the copy number of circDYM was estimated by absolute qPCR.

2.11 | EVs staining

As described in previous studies (Karimi et al., 2018; Pužar Dominkuš et al., 2018), EVs samples were stained and purified according to the following steps (Figure S2):

Step 1: Mock EVs or RVG-EVs were resuspended in particle-free Dulbecco's phosphate-buffered saline (DPBS, Sigma-Aldrich) to a protein concentration of 100 μg/ml. The resuspended EVs were then stained with Dil or DiR dye at 37°C for 15 min. Excess dye was bound with 10% EV-depleted foetal bovine serum. The EV samples were diluted with DPBS and pelleted by ultracentrifugation at 200,000 × *g* for 2 h at 4°C. The pellet was gently resuspended in 2 ml DPBS.

Step 2: EV samples were placed onto a 20%–60% discontinuous sucrose gradient. The gradient was ultracentrifuged at 10,000 × *g* for 18 h at 4°C using an XPN-100 ultracentrifuge (Beckman Coulter, USA). After that, fractions 7–10 were combined and diluted to 25 ml with DPBS. EVs were then pelleted by ultracentrifugation at 200,000 × *g* for 2 h at 4°C.

Step 3: Exo-spin™ buffer (EX03-8, Cell Guidance System, England) was added into the EV suspension with a 2:1 ratio. The resuspended EVs were transferred to a mini SEC column and centrifuged at 16,000 × *g* for 1 h in order to collect all liquid to the bottom of the tube. Finally, the pellets were gently resuspended in 100 μl DPBS.

2.12 | EVs uptake by primary mouse microglia

Vector-EVs, RVG-Vector-EVs, circDYM-EVs or RVG-circDYM-EVs at dosage of 200 μg resuspended in serum-free medium were added to primary mouse microglia at 37°C for 6 h. After incubation, the cells were washed three times with PBS to remove excess EVs and prepared for subsequent experiments.

2.13 | RVG-EVs dynamic uptake imaging

Primary mouse microglia (2×10^4 cells) were seeded in a 35 mm confocal dish. On the second day, Dil-labelled mock EVs or RVG-EVs were added into the cultured microglia, and then the confocal dish was placed in the living cell workstation (37°C, 5% CO_2). Next, the recorded cells were identified and the pictures were taken every 5 min for 6 h using a confocal microscope (FV3000, Olympus, Japan).

2.14 | Cell viability assessments

To evaluate the cytotoxicity of mock EVs or RVG-EVs in vitro, primary mouse microglia (approximately 1×10^5 cells) were seeded with 200 μg mock EVs or RVG-EVs in triplicate in a 96-well plate. After 6 h of cultivation, cell survival level was analysed using the CCK8 assay according to the manual (HY-K0301, MedChemExpress) on a microplate reader.

2.15 | Nitric oxide (NO) production assay

Primary mouse microglia (1×10^5 cells) were seeded in triplicate in a 24-well plate for 6 h co-incubation with 200 μg RVG-Vector-EVs or RVG-circDYM-EVs, and the cells then were treated with lipopolysaccharide (LPS) for 24 h. Thereafter, the culture supernatant was collected to measure NO production. On the basis of the Griess reaction, the NO production was determined using a commercial NO assay kit (S0021S, Beyotime) according to the manufacturer's instructions.

2.16 | Enzyme-linked immunosorbent assay (ELISA)

Cell culture supernatant was collected by centrifugation for 15 min at 1000 × *g*, 4°C. The tissue of hippocampus (100 mg) was rinsed and homogenized, and after three freeze-thaw cycles were performed to break the cell membranes, the supernatant was obtained by centrifugation for 5 min at 5000 × *g*, 4°C. The levels of cytokines (IL-6, IL-1β, MCP-1, and TNF-α) were analysed using commercial ELISA kits according to the manufacturer's instructions. The ELISA Kit of Mouse IL-6 (JEB-12267), Mouse IL-1β (JEB-12787), Mouse MCP-1 (JEB-15205), and Mouse TNF-α (JEB-12474) were purchased from Nanjing Jin Yibai Biological Technology Co. Ltd.

2.17 | Near infrared fluorescence (NIRF) imaging

DiR (22070, AAT Bioquest) was used to investigate biodistribution of mock EVs or RVG-EVs in vivo. For the targeting study, the mice were intravenously injected with DiR-labelled mock EVs or RVG-EVs at the dose of 200 μg. Then, the intensity and distribution of fluorescence were recorded at different time points (6, 12, 24 h) in vivo using an IVIS Spectrum Imaging System (PerkinElmer, USA). For in vitro imaging, the animals were sacrificed at 24 h after EVs administration by perfusion of saline, and the brain, heart, lungs, liver, spleen, and kidneys were dissected and fixed in 4% paraformaldehyde. The DiR fluorescence signals were analysed using Living Image 4.4 software (PerkinElmer, USA).

2.18 | Immunofluorescence staining and confocal imaging

Dil (C1036, Beyotime) was used to label EVs to investigate the cellular localization of the mock EVs or RVG-EVs at dosage of 200 μg in mouse brain. Next, Dil-labelled EVs were intravenously administered. Six hours later, the mice were perfused with 100 ml PBS and then 25 ml 4% PFA. The brain tissues were isolated and cut into 30 μm thickness. The sections were treated by 0.3% Triton X-100 (T109027, Aladdin) for 15 min and blocked with 10% normal goat serum (NGS, ZLI-9056, ZSGB-BIO) in 0.3% Triton X-100 for 1 h at room temperature. Next, the sections were immunostained with anti-HA (1:250, ab9110, Abcam), anti-Iba-1 (1:250, 019–19741, Wako Pure Chemicals), anti-GFAP (1:400, G3893, Sigma-Aldrich), or anti-NeuN (1:200, ab104224, Abcam) antibodies over night at 4°C. After washing three times with PBS, the samples were incubated with Alexa 647-conjugated goat anti-mouse IgG (1:300, AB_2535805, Invitrogen) or anti-rabbit IgG (1:300, AB_2535812, Invitrogen) for 1 h. After washing three times with PBS, the tissue sections were mounted onto glass slides. To explore the distribution of TAF1 in microglia, a rabbit anti-Iba-1 antibody (1:250, 019–19741, Wako Pure Chemicals) and a rabbit anti-TAF1 antibody (1:500, ab188427, Abcam) were used. The secondary antibody used was Alexa Fluor 488-conjugated Fab fragment goat anti-rabbit IgG (H + L) (1:400, 111-547-003, Jackson ImmunoResearch Laboratories) or Alexa Fluor 594 goat anti-rabbit IgG (1:300, A-11012, Invitrogen). Images were captured by confocal microscopy (FV3000, Olympus, Japan).

2.19 | Animals

Adult male C57BL/6J mice (24.0–26.0 g, 6–8 weeks old) were purchased from GemPharmatech (Nanjing, China). Prior to initiating experimental procedures, mice were randomly assigned to different groups and housed in 25 × 45 × 15 cm cages and maintained on a 12:12 h light/dark cycle (lights on at 07:00 AM). Food and water were available ad libitum. CUS mice were single-housed, and control mice were group-housed. All mice procedures were approved by the Institutional Animal Care and Use Committee of the Medical School, Southeast University.

2.20 | CUS protocol

Mice were exposed to various, randomly scheduled, low-intensity social-environmental stressors two times a day for 4 weeks. The stressors included (1) food or water deprivation for 24 h, (2) overnight illumination, (3) absence of sawdust in cage for 24 h, (4) moistened sawdust for 24 h, (5) forced swimming at 8°C for 5 min, (6) tail nipping (1 cm from the tip of the tail), (7) physical restraint for 6 h, and (8) 45° cage-tilt along the vertical axis for 3 h.

2.21 | Behavioural tests

Behavioural tests were carried out in a quiet and low-intensity environment and were scored by the same researcher. Mice were transferred to the testing room at least 3 h before behavioural tests, and the procedures were recorded by a video camera and analysed using a Plexon research solutions system (Plexon Inc, USA).

2.22 | Sucrose preference test (SPT)

SPT was used to test the preference of mice for sugar and evaluate anhedonia in mice. Briefly, one bottle of 1% (w/v) sucrose solution was supplied for 3 days to habituate mice to the solution. Then, mice were exposed to both tap water and sucrose solution bottles for 24 h to obtain the sucrose preference baseline. Finally, mice were subjected to a 24 h sucrose preference

test in which tap water and sucrose solution were provided by identical bottles. The positions of the two bottles were switched every 6 h, and sucrose and water consumptions were simultaneously measured. The preference to consume sucrose solution was calculated as percentage preference = [(sucrose intake/total intake) × 100]. Tests were performed by an individual blind to the animal's treatment status.

2.23 | Forced swim test (FST)

FST was carried out to assess depressive-like behaviours in mice. Mice were dropped individually into a clear Plexiglas cylinder (diameter: 20 cm; height: 25 cm) filled with 15 cm water maintained at 23–25°C. After some initial, vigorous activities in the water, mice tend to acquire an immobile posture, which is characterized by motionless floating with only necessary movements to keep their heads above water. After a 2-min habituation period, the duration of immobility was measured for 4 min. Tests were performed by an individual blind to the animal's treatment status.

2.24 | Tail suspension test (TST)

TST was used to test despair/depressive-like behaviours in mice. Mice were suspended from the ceiling of a box by adhesive tape that was placed approximately 1 cm below the tip of the tail. After a 2-min habituation period, immobility time was measured for 4 min. Tests were performed by an individual blind to the animal's treatment status.

2.25 | Open field test (OFT)

OFT was used to test the locomotor and exploratory behaviours in mice. The open-field apparatus was divided into sixteen equal squares. Mice were placed in the centre area. After a 2-min habituation period, the total movement distance, time spent in the centre, and the number of times mice cross the centre were recorded for 3 min. Tests were performed by an individual blind to the animals' treatment status.

2.26 | Intravenous delivery of circDYM in animals

C57BL/6J mice were anesthetized with 2% isoflurane and placed in a stereotactic apparatus. RVG-Vector-EVs or RVG-circDYM-EVs were intravenously administered to the mice. To determine tissue distribution of overexpressed circDYM in vivo, we harvested various tissues and monitored delivery efficiency by qPCR. CUS mice were selected from whose sucrose consumption were lower than the control's mean sucrose preference and immobile time in FST and TST were higher than the control's mean immobile time after 4 weeks CUS procedure. CUS mice were then grouped with control mice to evaluate the improvement of circDYM on depressive-like behaviours.

To explore the effect of different doses of circDYM mediated by RVG-EVs on depressive-like behaviours in CUS mice, we formed the following groups: Control + RVG-Vector-EVs (200 μg), Control + RVG-circDYM-EVs (200 μg), CUS +RVG-Vector-EVs (200 μg), CUS + RVG-circDYM-EVs (100 μg), CUS + RVG-circDYM-EVs (200 μg), CUS + RVG-circDYM-EVs (300 μg), and CUS + RVG-circDYM-EVs (400 μg).

To further confirm the effect of circDYM mediated by RVG-EVs on depressive-like behaviours in CUS mice, we formed the following groups: Control + RVG-Vector-EVs (200 μg), Control + RVG-circDYM-EVs (200 μg), CUS + RVG-Vector-EVs (200 μg), and CUS + RVG-circDYM-EVs (200 μg).

To explore the effect of RVG-HA polypeptides and mock EVs on depressive-like behaviours in CUS mice, we formed the following groups: Control + PBS, CUS + PBS, CUS + RVG-HA polypeptides (200 μg), CUS + mock EVs (200 μg), CUS +RVG-Vector-EVs (200 μg), and RVG-circDYM-EVs (200 μg).

2.27 | Splenic lymphocytes proliferation assay

RBC-depleted spleen cells were separated from the mice after 7 days of tail vein injection of 200 μg RVG-Vector-EVs or RVG-circDYM-EVs. Spleen cells were seeded into round-bottom 96-well plates in triplicate at 1×10^5 cells/well and co-incubated with 200 μg ml^{-1} RVG-Vector-EVs or RVG-circDYM-EVs. After 72 h of cultivation, cell proliferation was analysed on a microplate reader using the CCK8 assay according to the manual (HY-K0301, MedChemExpress).

2.28 | Flow cytometry (FCM)

Mice were deeply anaesthetized with 1% phenobarbital sodium and perfused transcardially with ice-cold PBS. Brains were rapidly removed and stored in ice-cold PBS. For cell analysis, brain tissues were digested by Papain (2 mg ml^{-1}, 3119, Worthington) in RPMI 1640 medium (61870044, Gibico) at 37°C. Cell suspension was then filtered through a 70-mm nylon mesh, and single cells were collected by centrifugation. The cells were resuspended in 30% Percoll density gradient (17-0891-09, GE Healthcare) and centrifuged for 25 min (900 × *g*, 25°C) at 4°C temperature. Cells were obtained by collection of the bottom fraction in 30% Percoll. Mouse microglia and astrocytes were then assayed for cell surface molecules. Briefly, cells were incubated for 15 min with Blocking Reagent (130-092-575, Miltenyi Biotec), and then stained with fluorochrome-conjugated antibodies or their corresponding isotopic controls for 30 min at 4°C in darkness. The following antibodies were used at the manufacturer's recommended dilutions: PE anti-mouse ACSA-2 (130-116-244, Miltenyi Biotec), APC anti-mouse/human CD11b (101212, BioLegend), and PerCp-Cy™5.5 anti-mouse CD45 (561869, BD Pharmingen).

To analyse leukocytes influxes following CUS treatment, cell suspension was obtained from mouse brain as mentioned above. Then cells were stained with PerCp-Cy™5.5 anti-mouse CD45 (550994, BD Pharmingen), PE-Cy7 anti-mouse Ly6G (127617, Biolegend), PE anti-mouse Ly6C (128007, Biolegend), PE anti-mouse CD3e (561824, BD Pharmingen), APC anti-mouse CD8a (553035, BD Pharmingen), APC-Cy7 anti-mouse CD4 (100413, Biolegend), or APC anti-human/mouse CD45R/B220 (07131-80-25, Biogems). To quantify peripheral myeloid infiltration, samples were gated for $CD45^+/CD3^+/CD4^+$ ($CD4^+$ T cells), $CD45^+/CD3^+/CD8^+$ ($CD8^+$ T cells), $CD45^+/B220^+$ (B cells), $CD45^+/Ly6G^+$ (neutrophils), $CD45^+/Ly6G^-/Ly6C^{low}$ (macrophages/monocytes), and $CD45^+/Ly6G^-/Ly6C^{hi}$ (macrophages/monocytes). All samples were measured using a NovoCyte flow cytometer (ACEA NovoCyte D2060R, Agilent Biosciences, USA). Data were analysed using NovoExpress Software version 1.4.0 (ACEA Biosciences, USA).

2.29 | Western blot

Lysates were harvested from cells in RIPA lysis buffer (P0013B, Beyotime) containing a protease inhibitor cocktail. Equal amounts of protein were separated via sodium dodecyl sulphate-polyacrylamide gel electrophoresis, and then transferred to polyvinylidene fluoride membranes electrophoretically. After incubation with blocking buffer, the membrane was incubated with antibodies against iNOS (1:1000, 18985-1-AP, Proteintech group), GFAP (1:5000, 60190-1-Ig, Proteintech group), ZO-1 (1:1000, 21773-1-AP, Proteintech group), Occludin (1:1000, 27260-1-AP, Proteintech group), Claudin-5 (1:1000, AF5216, Affinity), TAF1 (1:1000, 20260-1-AP, Proteintech group), Histone-H3 (1:1000, 17168-1-AP, Proteintech group), or GADPH (1:3000, 60004-1-AP, Proteintech group) overnight at 4°C. After three washes, the membrane was incubated with a horseradish peroxidase-conjugated goat anti-mouse/rabbit IgG secondary antibody (1:2000, 7076P2/7074P2, Cell Signaling). Signals were detected by Automatic Chemiluminescence Image Analysis System (Tanon 5200, Tanon Science & Technology). Quantification of the individual protein bands was performed via densitometry using Image J software.

2.30 | Immunohistochemistry and image analysis

Frozen sections (30 μm thickness) containing the intact hippocampus were prepared with a cryostat and incubated subsequently with 3% H_2O_2 for 10 min, 0.3% Triton X-100 for 15 min, and then blocked with 10% NGS in 0.3% Triton X-100 solution for 1 h at room temperature. Next, the sections were incubated with a rabbit anti-Iba-1 antibody (1:250, 019–19741, Wako Pure Chemicals) or anti-GFAP antibody (1:400, G3893, Sigma-Aldrich) overnight at 4°C. On the following day, the sections were washed and incubated with a biotinylated goat anti-rabbit IgG (1:250, BA-1000, Vector Laboratories) or a biotinylated goat anti-mouse IgG (1:250, BA-9200, Vector Laboratories) in PBS for 1 h at room temperature, and then incubated with VECTASTAIN® ABC Kit (PK-6200, Vector Laboratories) for 1 h. The horseradish peroxidase reaction product was visualized using an enhanced DAB peroxidase substrate kit (SK-4100, Vector Laboratories). Images were captured using a microscope (ImagerM2, Zeiss, Germany). Computer-based cell tracing software Neurolucida 360 (MBF Bioscience, USA) was used for three-dimensional (3D) reconstruction of Iba-1 or GFAP positive cells within the hippocampus. NeuroExplorer (MBF Bioscience, USA) was used to analyse 60 cells per animal. Sholl analysis was used to determine branch tree morphology by placing 3D concentric circles in 5 mm increments starting at 5 mm from the soma.

2.31 | Immunohistochemistry for Evans Blue (EB)

Perivascular marker isolectin B4 (Ib4) and intravascular Evans blue (EB, E2129, Sigma-Aldrich) staining was performed to evaluate whether BBB leakage occurred in mice after CUS treatment as previously described (Menard et al., 2017). Mice were

administered through the caudal vein 6 μl g^{-1} of body weight 2% (w/v) EB that was dissolved in saline. Ten minutes later, the mice were anesthetized with 1% (w/v) pentasorbital sodium and sacrificed, and the brains were obtained and fixed in 10 ml freshly prepared, cold 4% PFA + 0.05% glutaraldehyde. Next, the brains were cut into 40 μm thickness with a cryostat and subsequently incubated with biotinylated-Ib4 (1:50, L2140, Sigma-Aldrich) in $CaCl_2$-containing buffer and blocked with blocking solution (0.05% Triton X-100 and 2% NDS) at 4°C for 72 h. After three washes in PBS for 5 min, slices were incubated with streptavidin-FITC (1:250, 434311, Life Technology) secondary antibody. On the following day, the sections were washed three times again in PBS, and ProLong Gold Antifade Reagent containing DAPI was applied for the visualization of nuclei. Immunofluorescence images were captured by microscopy (FV3000, Olympus, Japan).

2.32 | RNA sequencing analysis

Whole RNA-sequencing analysis were completed by LC-Bio (Hangzhou, China). Briefly, primary mouse microglia from the Control + Vector group; Control + circDYM group; lipopolysaccharide (LPS, 100 ng ml^{-1}) + Vector group; and LPS + circDYM group were collected in TRIzol reagent. UMI technology was used to label each sequence fragment with sequence tags, which minimized the interference of duplication generated by PCR amplification on the quantitative accuracy of the transcriptome. RNA sequencing reads were aligned to the mouse genome (GRCh37/hg19) using the software Hisat2 (2.0.4). Transcript abundance was quantified as fragments per kilo base of exon per million fragments mapped (FPKM). The threshold of significantly differential expression was set at $P < 0.05$ and $|\log_2(\text{fold change})| \geq 1$. The Gene Expression Omnibus (GEO) accession code for the data in this manuscript number is GSE159904.

2.33 | RNA-binding protein immunoprecipitation (RIP)

RIP was performed with a Magna RIP™ RNA-binding protein immunoprecipitation kit (17-700, Millipore) according to the manufacturer's instructions. Briefly, cultured HEK 293T cells transfected with the cirDYM-GFP lentivirus for 72 h were collected with 0.5 ml lysis buffer. Next, magnetic beads were mixed with 5 μg of the antibody of TAF1 (ab188427, Abcam) in RIP washing buffer and incubated with rotation for at least 1 h at room temperature. Later, RIP lysates were incubated with the antibody-bound beads in RIP immunoprecipitation buffer overnight at 4°C. Finally, after the supernatant was discarded, the pellet was resuspended in the immunoprecipitated buffer containing proteinase K in tubes and placed them at 55°C for 30 min to digest the proteins. Purified RNAs were used to examine the expression of circDYM via qPCR.

2.34 | RNA pull-down assays

RNA pull-down assays were performed according to the manufacturer's instructions. 1×10^7 cells were lysed in 500 μl NP-40 lysis buffer (P0013F, Beyotime) and then incubated with 5′-biotinylated circDYM probe (5 μg, Invitrogen) against endogenous or ectopically expressed circDYM at room temperature for 3 h. Next, a total of 50 μl Streptavidin C1 magnetic beads (65002, Invitrogen) were added to each reaction tube and sequentially incubated at room temperature for another hour. Finally, the beads were washed five times with NP-40 lysis buffer, and enrichment of binding protein was tested by western blot. The 5′-biotinylated circDYM probe (5′-AAACGAGGGTTGTTTTCAAAAGAGTGGAGTATCAG-3′) was purchased from Invitrogen.

2.35 | Cytoplasmic and nuclear protein extraction

Cytoplasmic and nuclear protein extraction was performed using a commercial kit (P0028, Beyotime) following the manufacturer's instructions. Cells were harvested and suspended by equal volume solution A containing 1% PMSF, and cell lysates were mixed with 10 μl solution B by vortex and placed on ice for 1 min. Tissue sample fragments were homogenized with a mixture of solutions A and B by a glass homogenizer. Supernatant (cytoplasmic protein) was obtained after 12,000 rpm centrifugation for 5 min; 50 μl solution C was used to suspend the sediment. Samples were mixed by vortex for 30 s every 2 min for 15 times, and supernatant (nuclear protein) was collected after centrifugation.

2.36 | Fluorescence in situ hybridization (FISH)

Primary mouse microglia plated on coverslips were permeabilized with 0.25% Triton X-100 for 15 min at room temperature followed by hybridization with 500 nM of a biotinylated circDYM probe overnight at 37°C. On the following day, coverslips

were washed five times and then blocked with a mixture solution of 1% BSA (BS043D, Biosharp) and 3% NGS for 1 h at room temperature. Next, cells were incubated with streptavidin-FITC (1:250, 434311, Life Technology) secondary antibody in PBS overnight at 4°C. After completion of the in situ hybridization, coverslips were blocked with 1% BSA/1% Triton X-100 in PBS (w/v for BSA and v/v for Triton X-100) for 1 h at room temperature and then incubated with a rabbit anti-TAF1 antibody (1:500, ab188427, Abcam) for 24 h. Coverslips were washed three times in PBS and incubated with Alexa Fluor 594 goat anti-rabbit IgG (1:250, A-11012, Invitrogen). Finally, coverslips were washed three times and mounted on slides with DAPI solution (0100-20, SouthernBiotech).

2.37 | Chromatin immunoprecipitation (ChIP) assay

The ChIP assay was performed according to the manufacturer's instructions (P2078, Beyotime). Briefly, fresh formaldehyde was added directly to the medium for cross-linking, and the final concentration of formaldehyde was 1%. After 10 min of incubation at room temperature, the unreacted formaldehyde was quenched with 10× glycine for 5 min at room temperature. Washed cells were scraped with cold PBS containing 1 mM PMSF and then centrifuged (1000 × *g*, 2 min, 4°C) to pellet the cells. Nuclei were harvested from the cell pellet using SDS lysis buffer containing 1 mM PMSF. DNA was sheared by sonication. The sheared, cross-linked chromatin was then diluted with Protein A + G Agarose/Salmon Sperm DNA and incubated for 30 min. After centrifugation, the sheared, cross-linked chromatin was mixed with antibodies for TAF1 (ab188427, Abcam), Histone H3 (9715s, Cell Signaling), and IgG (2729, Cell Signaling) and allowed to incubate overnight at 4°C. After the cross-linked protein/DNA complexes were washed with a series of cold wash buffers (including a low-salt buffer, a high-salt buffer, an LiCl buffer, and finally, a TE buffer), the complexes were reversed to free the bound DNA with elution buffer and purified using DNA purification spin columns. Finally, the purified DNA was amplified via PCR to identify the promoter region containing the specific binding site. The primer sequences are listed in Table S4.

2.38 | Statistical analysis

Statistical analysis was performed using GraphPad Prism 8.0.2 Software (GraphPad Software, USA). Significance was assessed with a two-tailed Student's *t* test for comparisons of two groups. Brown-Forsythe test was firstly used to evaluate the homogeneity of variance. One/Two-way ANOVA followed by the Holm-Sidak test were used for multi-group (three or more) comparisons. All data were presented as mean ± SEM. The statistical analysis used for the different experiments are described in the respective figure legends, and results were considered to be statistically significant if P was < 0.05.

3 | RESULTS

3.1 | Preparation and characterization of engineered RVG-EVs

For targeted in vivo delivery of circDYM to the brain without BBB restriction, we generated RVG-circDYM-EVs according to a previous publication (Alvarez-Erviti et al., 2011). RVG peptide that specifically binds to AChR were cloned into Lamp2b to confer neuronal cells targeting capabilities. Moreover, the amino acid sequence GNSTM was fused to the N terminus of RVG-Lamp2b-HA to protect fused proteins from proteolytic degradation. Then, the plasmid encoding the GNSTM-3-RVG-10-Lamp2b-HA polypeptide and the vector or overexpressed circDYM-GFP lentivirus were co-transfected to HEK 293T cells, and then RVG-EVs were collected by gradient centrifugation (Figure 1a). Next, isolated RVG-EVs were verified by TEM, NTA, and western blot analysis. RVG-EVs were physically homogenous when observed under TEM, with size peaking at 115.2 nm in diameter as determined by NTA (Figure 1b,c). Western blot analysis of characteristic EV membrane proteins, HA, Lamp2b, CD63, TSG101, and GM130 further confirmed the identity of the RVG-EVs (Figure 1d).

Attesting to the purity of the prepared RVG-EVs, the Histone-H3 levels detected with western blot were extremely low (Berda-Haddad et al., 2011) (Figure S3). We next used absolute qPCR to assess the circDYM production in HEK 293T cells transfected with a lentiviral expression vector. As shown in Figure 1e, there was 2.29 copies of circDYM per nanogram of RNA in RVG-Vector-HEK 293T cells group (likely representing the endogenous expression level of human circDYM), while there were 1447.57 copies of circDYM per nanogram of RNA in RVG-circDYM-HEK 293T cells. Additionally, the copy number of circDYM was 0.17 in each of RVG-Vector-EV, while the copy number of circDYM is 34.75 in each of RVG-circDYM-EV (Figure 1f). Moreover, we found that circDYM is protected within intact EVs as evidenced by the fact that treatment of RVG-circDYM-EVs with RNase A/T1 mix did not reduce the level of circDYM, unless we co-treated the RVG-circDYM-EVs with 1% Triton X-100, which degrades EV membranes (Figure 1g). In addition, as shown in Figure S4, RNase R treatment did not affect the yields of circDYM extracted from RVG-circDYM-EVs.

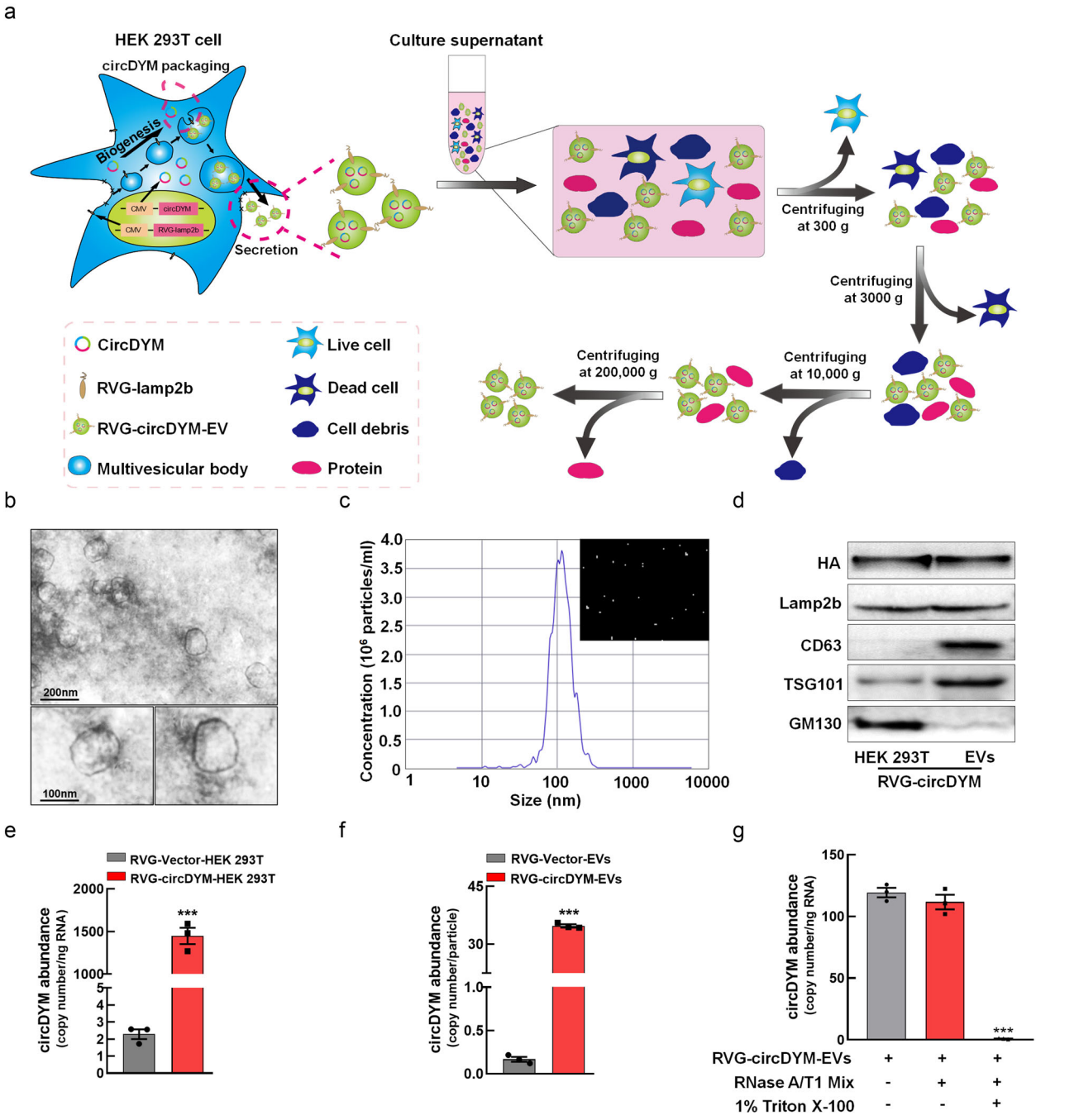

FIGURE 1 Preparation and characterization of engineered RVG-EVs. (a) Schematic diagram of the production and harvest of engineered RVG-EVs for targeted circDYM delivery. (b) TEM of RVG-EVs isolated from the culture medium of HEK 293T cells. (c) RVG-EVs were measured by NTA. (d) Western blot analysis of HA, Lamp2b, CD63, TSG101, and GM130 from RVG-circDYM-HEK 293T cells and RVG-circDYM-EVs. (e) Absolute qPCR analysis of circDYM copy numbers in HEK 293T cells transduced with vector or circDYM lentivirus. ***$P < 0.001$ versus the RVG-Vector-HEK 293T cells group using Student's *t*-test. (f) Absolute qPCR analysis of circDYM copy numbers in RVG-circDYM EVs. ***$P < 0.001$ versus RVG-Vector-EVs using Student's *t*-test. (g) Absolute qPCR analysis of circDYM copy numbers in RVG-EVs after treatments with RNase A/T1 Mix and 1% Triton X-100 for 30 min. ***$P < 0.001$ versus the Control group using one-way ANOVA followed by Holm-Sidak post hoc multiple comparisons test. All data were presented as mean ± SEM of three independent experiments. Images of unedited full blots in Figure S16

3.2 | RVG-circDYM-EVs inhibited primary mouse microglial activation in vitro

To investigate the role of RVG-circDYM-EVs in vitro, mock EVs, Vector-EVs, circDYM-EVs, RVG-Vector-EVs or RVG-circDYM-EVs were successfully prepared, and then were co-incubated with primary mouse microglia. It is worth noting that microglia contain AChR that binds to RVG and promotes uptake of RVG-EVs according to previous studies (Chivero et al., 2020)

(Figure 2a, Kim et al., 2010). In our study, AChR α7 siRNA was applied to examine whether AChR facilitated the internalization of RVG-EVs in primary mouse microglia (Figure S5a). As shown in Figure S5b, the knockdown of AChR significantly inhibited the internalization of RVG-EVs in primary microglia as determined by the reduced circDYM levels. Then, the dynamic uptake processes of mock EVs and RVG-EVs at different time points in vitro were observed using a live cell imaging system. As shown in Figure 2b and Movie 1 and 2, with the increase of co-incubation time, Dil-labelled RVG-EVs (red fluorescence) in primary microglia gradually increased. Moreover, the aggregation rate and intensity of red fluorescence in the RVG-EVs group were significantly higher than that of mock EVs (Figure 2c). In addition, the in vitro uptake effect of Dil-labelled RVG-EVs were also confirmed by using fluorescent microscopy. As shown in Figure S6, Dil-labelled RVG-EVs (red fluorescence) were internalized by primary microglia (lake blue fluorescence) after 6 h co-incubation. Then, we sought to evaluate whether mock EVs or RVG -EVs affect viability of primary microglia. CCK8 assay was performed and demonstrated that both mock EVs and RVG-EVs had no obvious toxic effect on primary microglia (Figure 2d). Absolute qPCR revealed that RVG-circDYM-EVs significantly increased the level of circDYM in primary microglia compared with circDYM-EVs after co-incubation with primary microglia for 6 h (Figure 2e). Then, to explore the effect of RVG-circDYM-EVs in the activation of primary microglia, western blot, nitrite assay and ELISA assay were conducted. As shown in Figure 2f, western blot revealed RVG-circDYM-EVs significantly decreased the increased iNOS expression induced by LPS in primary microglia. The effect of RVG-circDYM-EVs on microglial activation was further confirmed as indicated by NO levels (Figure 2g) and pro-inflammatory cytokines production (IL-6, IL-1β, MCP-1 and TNF-α; Figure 2h–k) using nitrite and ELISA assay, respectively.

3.3 | Biodistribution of DiR-labelled RVG-EVs in vivo

Having determined the uptake and function of RVG-EVs in microglia in vitro, we next sought to track the biodistribution of RVG-EVs in vivo. DiR-labelled mock EVs or RVG-EVs at the dosage of 200 μg were injected into mice via the tail vein, and an in vivo imaging system (IVIS) was employed. As shown in Figure 3a, the intensity and distribution of fluorescence were recorded at different time points (6, 12, 24 h) after mock EVs or RVG-EVs injection. According to the fluorescence quantification of different organs (brain, heart, liver, spleen, lung, and kidney), the fluorescence intensity was most obviously concentrated in the peripheral organs at 24 h after mock EVs or RVG-EVs injection, with the most obvious accumulation in the liver (Figure 3b,c). Then, the ability of RVG-EVs to deliver circDYM in vivo was assessed by absolute qPCR, which detected the abundance of circDYM in various organs of mice at different time points (2, 6, 12, and 24 h) after circDYM-EVs or RVG-cirDYM-EVs injection. As shown in Figure 3d,e, circDYM were found to be enriched in various organs at different post-injection time points. Moreover, circDYM expression in the liver was the highest among all organs within 6 h after administration, and overexpressed circDYM expression were sharply decreased in peripheral organs with time. However, the level of circDYM in the brain decreased slowly over time and was relatively stable compared to peripheral organs. Notably, absolute qPCR revealed a higher expression of circDYM in the brain treated with RVG-circDYM-EVs than circDYM-EVs (Figure 3d,e).

3.4 | Engineered RVG-EVs efficiently delivered exosomal circDYM into the brain

Next, to confirm the ability of RVG-EVs to target the brain, the entry of DiR-labelled mock EVs or RVG-EVs at the dosage of 200 μg into the brain was also monitored using IVIS. As shown in Figure 4a,b, the fluorescence intensity in brain regions was significantly higher for the RVG-EVs than for mock EVs at different time points (6, 12, 24 h) after mock EVs or RVG-EVs injection, thereby confirming a brain-targeting functional impact from the RVG glycoprotein that we used to modify the EVs. Since the C-terminal of the fusion protein RVG-Lamp2b that modifies EVs contains the HA label, anti-HA antibody can be used to confirm the location of RVG-EVs in brain. As shown in Figure 4c, the lake blue signal of HA tag-stabilized peptide-RVG fusion proteins co-localized with the red signal of Dil staining in the hippocampus of the mice at 6 h after injection, while there was no co-localization for mock EVs, which verified the reliability of Dil-labelled RVG-EVs. Moreover, co-localization of Dil^+ RVG-EVs and immunofluorescent markers for microglia (Iba-1) in the hippocampus of the mice supported that the RVG-EVs successfully targeted to microglia (Figure 4d). We also detected Dil-labelled RVG-EVs with astrocytes (GFAP), and neurons (NeuN) (Figure S7). Then, to verify the effectiveness of engineered RVG-EVs to deliver circDYM into hippocampus of the brain, absolute qPCR was conducted. The result showed that RVG-circDYM-EVs administration also significantly increased the level of circDYM in hippocampus tissues 24 h after EVs administration (Figure 4e).

3.5 | Effects of different doses of circDYM-RVG-EVs on depressive-like behaviours in CUS mice

To further investigate the efficiency of engineered RVG-EVs to deliver circDYM in vivo, mice were injected once intravenously with different doses of RVG-circDYM-EVs, and circDYM levels in the brain were assayed after 24 h. As shown in Figure 5a,

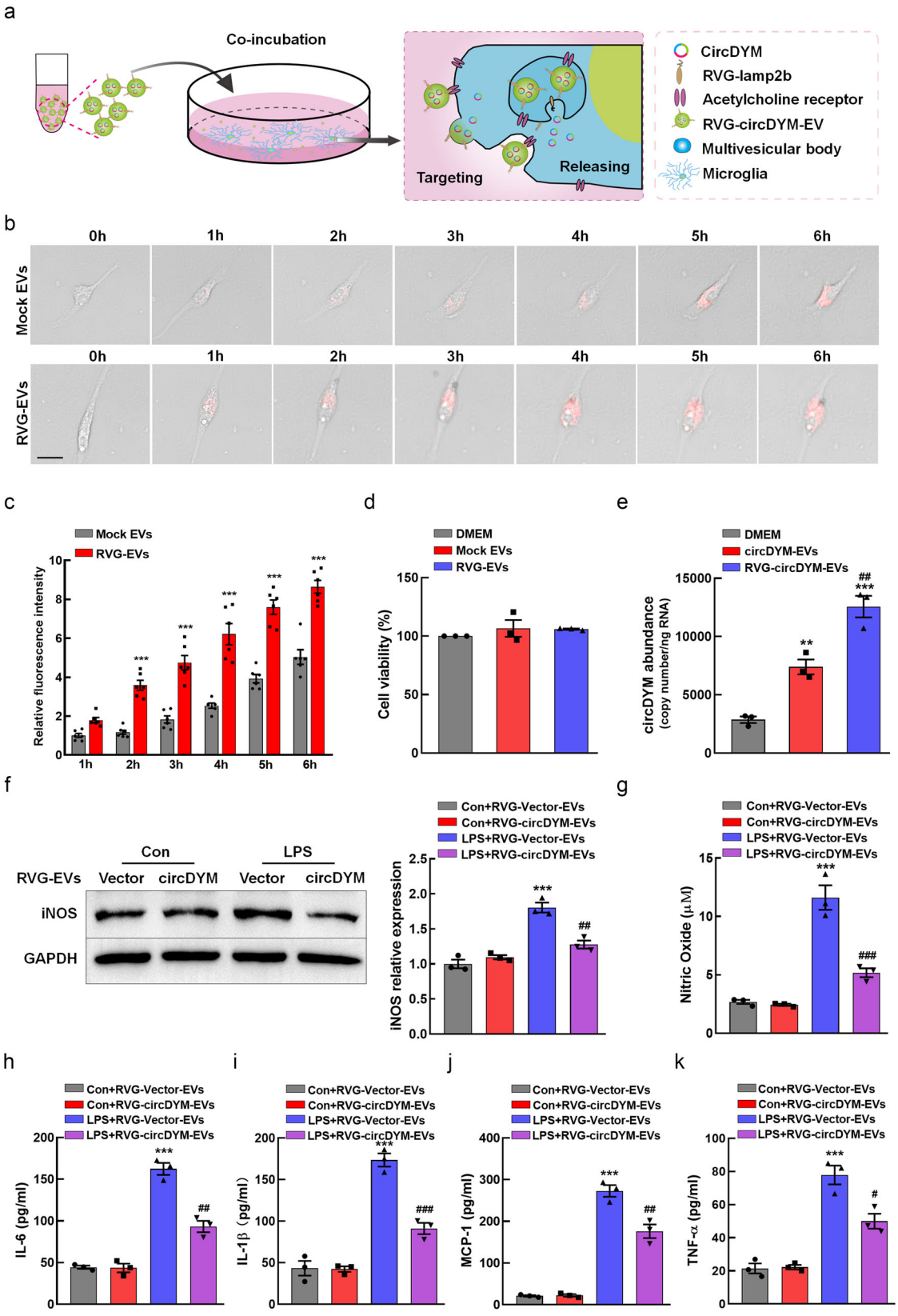

FIGURE 2 RVG-circDYM-EVs inhibited primary mouse microglial activation in vitro. (a) Schematic illustration of the addition and uptake of engineered RVG-EVs into the primary mouse microglia. (b) Bright-field images of primary mouse microglia incubated with mock EVs or RVG-EVs at 0, 1, 2, 3, 4, 5, and 6 h. Scale bar: 20 μm. (c) Quantitative fluorescence analysis of Dil in primary mouse microglia after incubation with Dil-labelled mock EVs or RVG-EVs ($n = 6$ for each group). $^{***}P < 0.001$ versus the mock EVs group using two-way repeated-measures ANOVA followed by the Holm-Sidak post hoc multiple comparison test. (d) CCK8 assay was performed after primary mouse microglia were incubated with mock EVs or RVG-EVs for 6 h. (e) Absolute qPCR analysis of circDYM copy numbers in primary mouse microglia after co-incubation with circDYM-EVs or RVG-circDYM-EVs for 6 h. $^{**}P < 0.01$, $^{***}P < 0.001$

different doses of RVG-circDYM-EVs increased the copy number of circDYM in a dose-dependent manner. Then, to discern the effects of RVG-circDYM-EVs on CUS mice, the mice exposed to the CUS protocol for 4 weeks with depressive-like behaviours were selected as subsequent subjects through depressive-like behavioural tests. Then, the selected CUS mice were intravenously administered different doses of RVG-Vector-EVs or RVG- circDYM-EVs daily for 7 days. Finally, depressive-like behavioural tests were conducted (Figure 5b). As shown in Figure 5c–e, RVG-circDYM-EVs administration of 200 μg, 300 μg and 400 μg, but not 100 μg, had an increased sucrose preference in comparison to RVG-Vector-EV-treated mice. In both FST and TST, immobility time was significantly extended in CUS mice, which was significantly decreased in 200 μg, 300 μg and 400 μg RVG-circDYM-EV-treated mice. In addition, 200 μg, 300 μg, and 400 μg RVG-circDYM-EV-treated mice exhibited more interest in exploring the central region and in locomotion compared with the CUS group in the OFT test (Figure 5f–h). Since 200 μg RVG-circDYM-EVs and above alleviated depressive-like behaviours in CUS mice, 200 μg RVG-circDYM EVs was used as the lowest therapeutic dose.

3.6 | RVG-EV-mediated delivery of circDYM alleviated depressive-like behaviours in CUS mice

To further confirm the therapeutic effect of 200 μg RVG-circDYM-EVs on CUS mice, the number of mice in each group was increased to 12 (Figure S8a). We found that circDYM was decreased in the hippocampus of CUS mice while intravenously administered RVG-circDYM-EVs significantly increased the expression of circDYM (Figure S8b). As shown in Figure 8c–h, CUS mice administered RVG-circDYM-EVs significantly ameliorated depressive-like behaviours induced by CUS. Based upon this finding, we concluded that the amount of circDYM released from 200 μg RVG-circDYM-EVs is able to induce the maximal detectable pharmacological effect on these depressive model mice.

To exclude the effect of RVG-HA polypeptides and mock EVs on depressive-like behaviours in CUS mice, we added RVG-HA and mock EVs groups (Figure 6a). Prior to the behavioural tests in mice, immunofluorescence staining showed that RVG-HA reached the brain through the BBB (Figure S9). As shown in Figure 6b, 200 μg RVG-circDYM-EV administration significantly increased the decreased sucrose intake in CUS mice, while RVG-HA did not increase the decreased sucrose intake of CUS mice. Similarly, RVG-circDYM-EV administration decreased the increased immobility time of CUS mice. However, treatment with RVG-HA or mock EVs did not decrease the increased immobility time of CUS mice (Figure 6c,d). Moreover, mice injected with RVG-HA or mock EVs did not exhibit interest in exploring the central region or in locomotion compared with the CUS group in the OFT test (Figure 6e–g). Based on the above findings, we ruled out the possibility that RVG-HA or mock EVs contributed to the alleviation of depressive behaviours in mice.

In addition, in order to exclude any possible RVG-HA, mock EVs, or RVG-EVs induced immune responses, we performed FCM to assess $CD4^+$ T cells, regulatory T (Treg) cells, and Th17 cells in the peripheral blood of mice after 7 days of 200 μg RVG-HA, mock EV, or RVG-EV treatment. As shown in Figure 6h, there was no significant change in the number of peripheral immune cells after RVG-HA, mock EV, RVG-Vector-EV, or RVG-circDYM-EV injection, suggesting that RVG-HA, mock EVs, and RVG-EVs didn't induce obvious immune rejection in vivo. Moreover, a CCK8 proliferation assay was performed to verify that no T cell proliferation was triggered in a mixed splenocyte reaction after 7 days of RVG-HA, mock EV, RVG-Vector-EV, or RVG-circDYM-EV treatment (Figure S10). These experiments suggested that RVG-EVs harvested from HEK 293T cells were well tolerated in vivo from an immunological standpoint.

3.7 | RVG-EV-mediated delivery of circDYM attenuated microglial activation

Since RVG-circDYM-EV treatment was effective in alleviating depressive-like behaviours of CUS mice, we next explored the cellular mechanisms involved in this process. Central nervous system (CNS) inflammation is considered one of the main triggers of depression (Miller & Raison, 2016; Wang et al., 2018) with IL-6, IL-1β, MCP-1, and TNF-α being major proinflammatory cytokines produced in the CNS. As shown in Figure 7a–d, RVG-circDYM-EV treatment significantly reduced CUS-induced inflammatory response in the hippocampus as indicated by decreased production of IL-6, IL-1β, MCP-1, and TNF-α. Moreover,

versus the Control group; $^{\#\#}P < 0.01$ versus the circDYM-EVs group using one-way ANOVA followed by Holm-Sidak post hoc multiple comparisons test. (f) Representative western blots of iNOS levels in primary mouse microglia after 6 h co-incubated with RVG-Vector-EVs or RVG-circDYM-EVs with or without LPS treatment. $^{***}P < 0.001$ versus the Control + RVG-Vector-EVs group; $^{\#\#}P < 0.01$ versus the LPS + RVG-Vector-EVs group using two-way ANOVA followed by the Holm-Sidak post hoc multiple comparison test. (g) NO production in primary mouse microglia after 6 h co-incubated with RVG-Vector-EVs or RVG-circDYM-EVs with or without LPS treatment. $^{***}P < 0.001$ versus the Control + RVG-Vector-EVs group; $^{\#\#\#}P < 0.001$ versus the LPS + RVG-Vector-EVs group using two-way ANOVA followed by the Holm-Sidak post hoc multiple comparison test. (h–k) Level of IL-6 (h), IL-1β (i), MCP-1 (j), and TNF-α (k) measured by ELISA in primary mouse microglia after 6 h co-incubated with RVG-Vector-EVs or RVG-circDYM-EVs with or without LPS treatment. $^{***}P < 0.001$ versus the Control + RVG-Vector-EVs group; $^{\#}P < 0.05$, $^{\#\#}P < 0.01$, $^{\#\#\#}P < 0.001$ versus the the LPS + RVG-Vector-EVs group using two-way ANOVA followed by the Holm-Sidak post hoc multiple comparison test. Images of unedited full blots in Figure S17

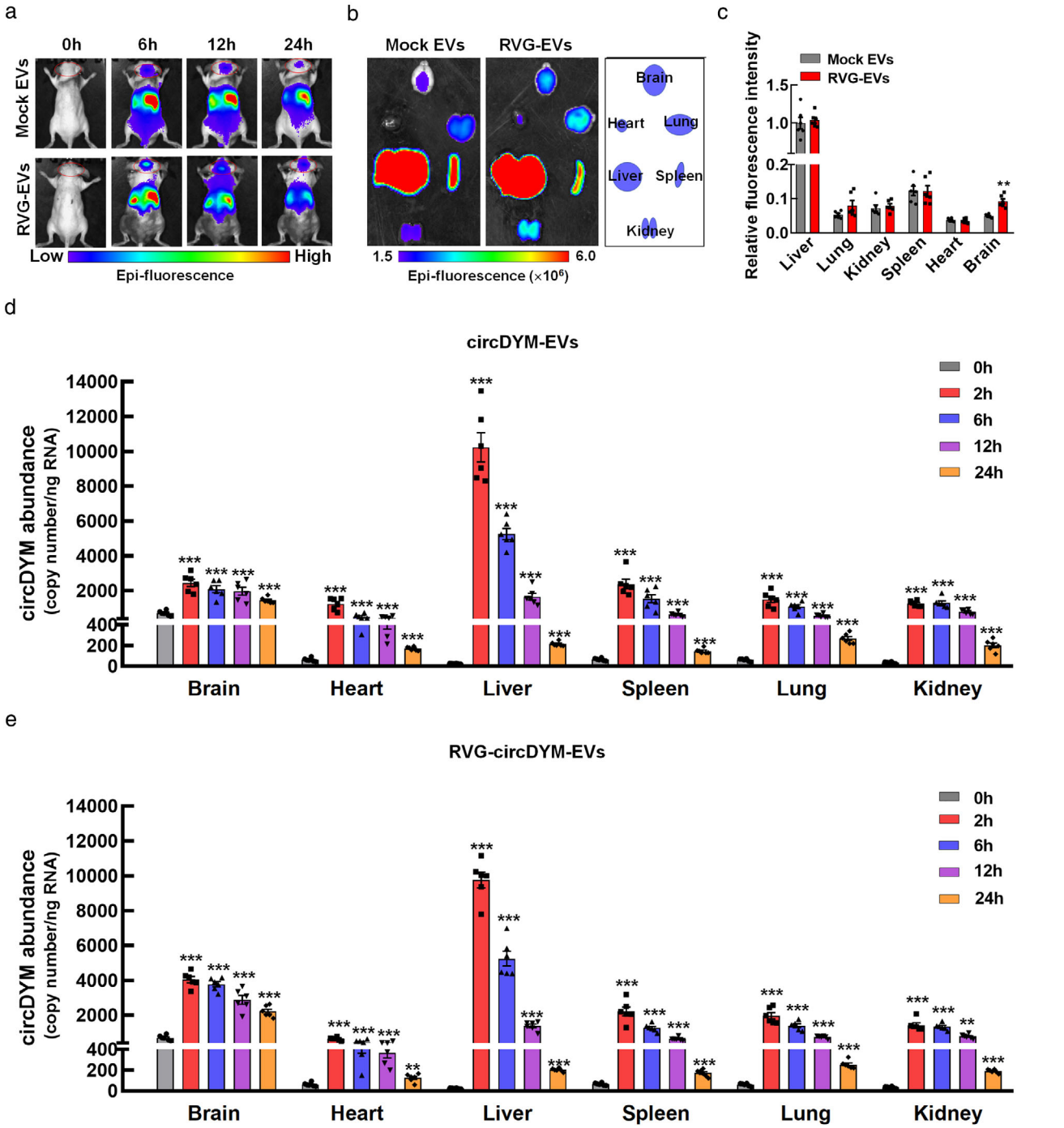

FIGURE 3 Biodistribution of DiR-labelled RVG-EVs in vivo. (a) Representative live fluorescence imaging of DiR-labelled mock EVs or RVG-EVs distribution in the mice. (b) Distribution of mock EVs or RVG-EVs in different organs of the mice after 24 h of injection. Right boxed graph illustrates location of the analysed six organs. (c) Quantitation of fluorescence intensities in different organs. $^{**}P < 0.01$ versus the mock EVs group using Student's *t*-test. (d) qPCR analysis of circDYM levels in the brain, heart, liver, spleen, lung, and kidney of normal mice at h 2, 12 and 24 after intravenous injection of circDYM-EVs with a dose of 200 μg ($n = 6$ for each group). $^{***}P < 0.001$ versus the untreated group using one-way ANOVA followed by the Holm-Sidak post hoc multiple comparison test. (e) qPCR analysis of circDYM levels in the brain, heart, liver, spleen, lung, and kidney of normal mice at h 2, 12 and 24 after intravenous injection of RVG-circDYM-EVs with a dose of 200 μg ($n = 6$ for each group). $^{**}P < 0.01$, $^{***}P < 0.001$ versus the untreated group using one-way ANOVA followed by the Holm-Sidak post hoc multiple comparison test

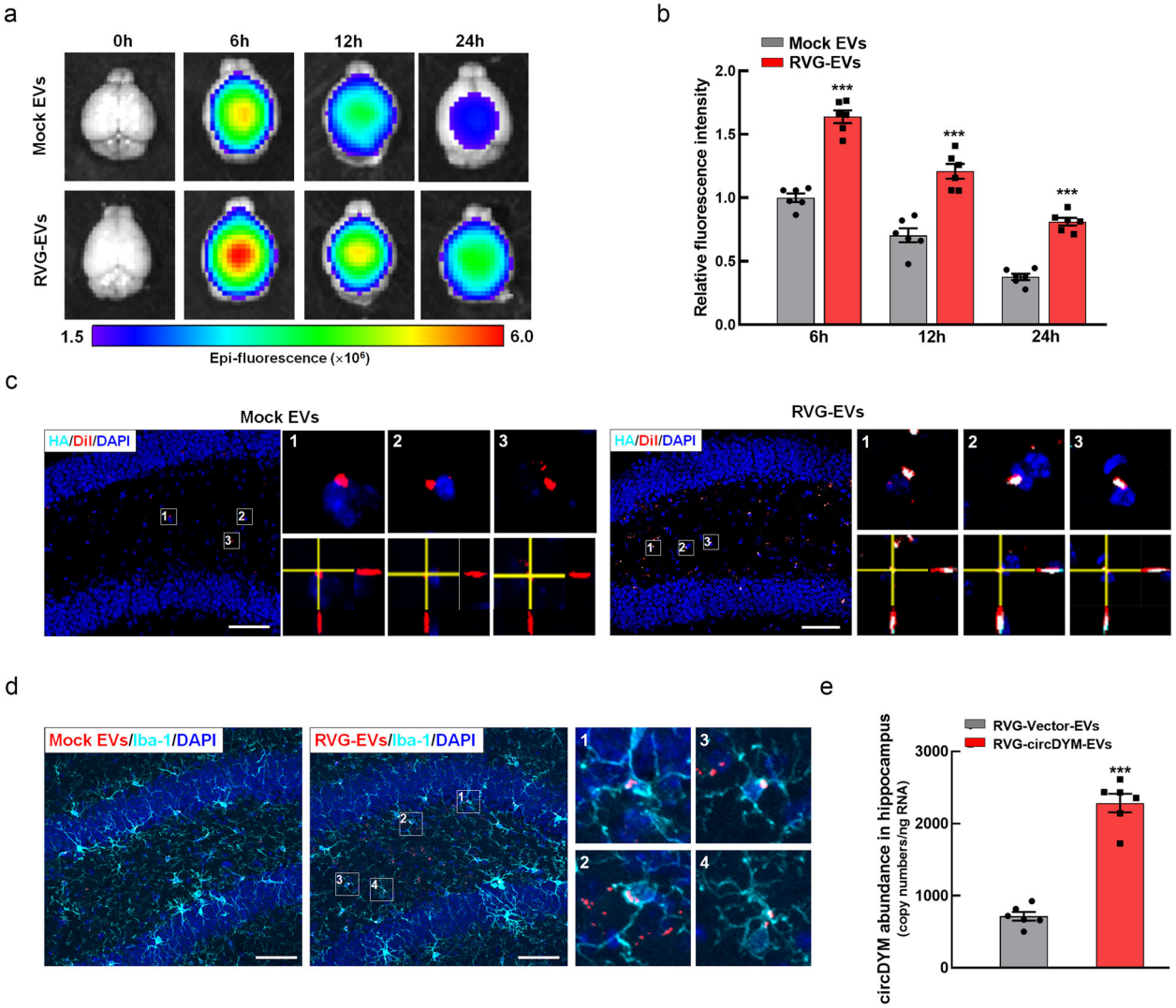

FIGURE 4 Engineered RVG-EVs efficiently delivered exosomal circDYM into the brain. (a) Representative NIRF images of mice brains which received the administration of DiR-labelled mock EVs or RVG-EVs. (b) Quantitation of fluorescence intensity in the brains. ***$P < 0.001$ versus the mock EVs group using two-way ANOVA followed by the Holm-Sidak post hoc multiple comparison test. (c) Co-localization of Dil-labelled mock EVs or RVG-EVs and HA tag-stabilized peptide-RVG fusion proteins in the brain of normal mice. Scale bar: 50 μm. (d) Confocal microscopy images of Dil-labelled mock EVs or RVG-EVs. Red fluorescent spots indicate Dil-labelled EVs, and lake blue fluorescence represents Iba-1 (microglia). Scale bar: 50 μm. (e) Absolute qPCR analysis of RNA extracted from the mouse hippocampus 24 h after injection of RVG-Vector-EVs or RVG-circDYM-EVs ($n = 6$ for each group). ***$P < 0.001$ versus the RVG-Vector-EVs group using Student's t-test

western blot revealed that the expression of iNOS was significantly decreased in the hippocampus of CUS mice treated with RVG-circDYM-EVs compared with RVG-Vector-EV-administered animals (Figure 7e). Because microglia are the primary regulators of neuroinflammation, microglial cells in brains were then isolated via the Percoll gradient method and assessed by FCM. As shown in Figure 7f, RVG-circDYM-EV treatment decreased the percentage of $CD11b^{+}CD45^{dim}$ cell population (microglia) in CUS mice. This finding was confirmed by immunohistochemistry as RVG-circDYM-EV treatment significantly inhibited microglial activation by decreasing microglial soma size, branch number, branch length and branch volume (Figure 7g–k) in the hippocampus of CUS mice.

Astrocytes are key players in sensing homeostatic disturbances in the CNS, and CUS mice suffer from astrocyte dysfunction (Cao et al., 2013). Western blot revealed that RVG-circDYM-EV treatment significantly inhibited the decreased expression of GFAP in the hippocampus of CUS mice (Figure S11a). Brain astrocytes were then isolated to be assessed by flow cytometry, and RVG-circDYM-EV treatment notably increased the percentage of $ASCA\text{-}2^{+}$ cell population (astrocytes) in the brain of CUS mice (Figure S11b). Similarly, immunohistochemistry confirmed that RVG-circDYM-EV treatment significantly attenuated astrocyte dysfunction, as indicated by the increased GFAP-positive cells and ramification of astrocytes, characterized by significantly increased branch number, volume, and length (Figure S11c–g), in the hippocampus of RVG-circDYM-EV treated mice.

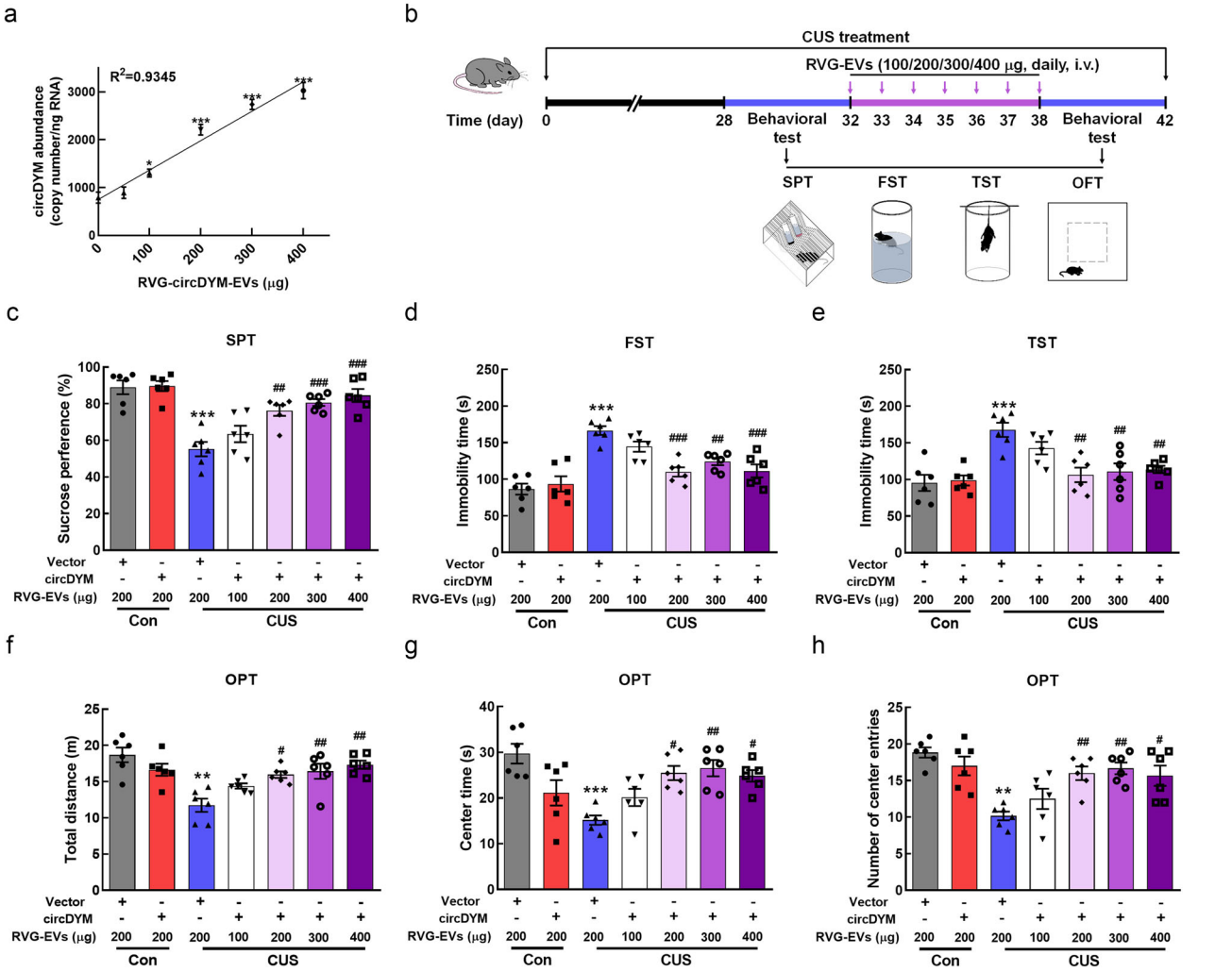

FIGURE 5 Effects of different doses of circDYM mediated by RVG-EVs on depressive-like behaviours in CUS mice. (a) qPCR analysis of circDYM levels in the brain of normal mice following injection of various quantities of RVG-circDYM-EVs ($n = 3$ for each group). $^{*}P < 0.05$, $^{***}P < 0.001$ versus the untreated group using one-way ANOVA followed by the Holm-Sidak post hoc multiple comparison test. (b) Schematic of the experimental procedure and behavioural studies. (c–h) CircDYM relieved depressive-like behaviours in CUS mice ($n = 6$ for each group) as measured by the SPT (c), FST (d), TST (e) and OFT (f–h). $^{**}P < 0.01$, $^{***}P < 0.001$ versus the Control + RVG-Vector-EVs group; $^{\#}P < 0.05$, $^{\#\#}P < 0.01$, and $^{\#\#\#}P < 0.001$ versus the CUS + RVG-Vector-EVs group using two-way ANOVA followed by the Holm-Sidak post hoc multiple comparison test

3.8 | RVG-EV-mediated delivery of circDYM reduced CUS-induced BBB damage and infiltration of peripheral immune cells

The BBB is a dynamic interface between the brain and blood circulation, and the loss of BBB integrity is a pathological finding in psychiatric disorders (Menard et al., 2017). To investigate whether RVG-circDYM-EVs can regulate cerebrovascular integrity, we examined the expression of tight junction proteins (TJPs), including ZO-1, Occludin and Claudin-5. As shown in Figure S12a–c, the expression of TJPs notably decreased in the hippocampus of CUS mice, which was rescued by RVG-circDYM-EV treatment. EB dye, which has a very high affinity for serum albumin, was used to confirm this finding. RVG-circDYM-EVs dramatically decreased the infiltration of EB in the hippocampus of CUS mice compared to the CUS + RVG-Vector-EVs group; the dye accumulated in the perivascular space of hippocampus blood vessels but not in the brain parenchyma (Figure S12d).

Due to CUS-induced neurovascular damage and increased BBB permeability, we hypothesize that peripheral immune cells could diffuse into the brain of CUS mice. To examine this possibility, we collected $CD45^{+}$ bone marrow-derived cells from the mouse brain, and FCM was used to quantify lymphoid and myeloid cell populations (Figure S12e). As shown in Figure S12f–k, FCM revealed more $CD4^{+}$ T cells (Figure S12f), $CD8^{+}$ T cells (Figure S12g), $B220^{+}$ B cells (Figure S12h), $Ly6G^{-}Ly6C^{low}$ macrophages/monocytes (Figure S12i) in the brain of CUS mice, and the infiltration of these peripheral immune cells was significantly decreased by RVG-circDYM-EV treatment. There was no difference between CUS + RVG-Vector-EVs and CUS + RVG-circDYM-EVs groups in $Ly6G^{-}Ly6C^{hi}$ macrophages/monocytes (Figure S12j) or $Ly6G^{+}$ neutrophils (Figure S12k). In brief,

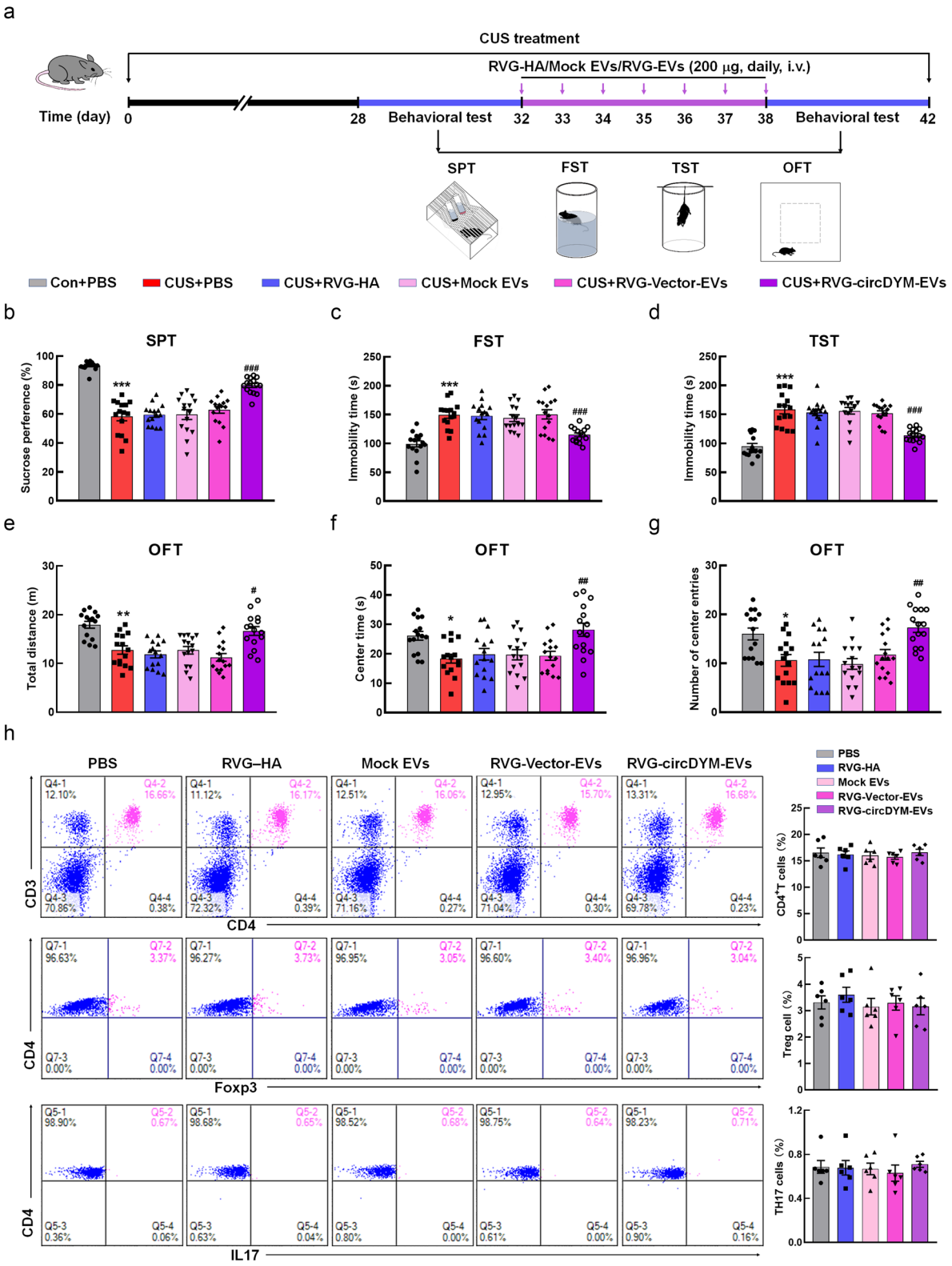

FIGURE 6 RVG-EV-mediated delivery of circDYM alleviated depressive-like behaviours in CUS mice. (a) Schematic of the experimental procedure and behavioural studies. (b–g) CircDYM relieved depressive-like behaviours in CUS mice ($n = 6$ for each group) as measured by the SPT (b), FST (c), TST (d) and OFT (e–g). $^{*}P < 0.05$, $^{**}P < 0.01$, $^{***}P < 0.001$ versus the Control + RVG-Vector-EVs group; $^{\#}P < 0.05$, $^{\#\#}P < 0.01$, and $^{\#\#\#}P < 0.001$ versus the CUS + RVG-Vector-EVs group using two-way ANOVA followed by the Holm-Sidak post hoc multiple comparison test. (h) Peripheral immune cells analysed by FCM indicated no overt changes in $CD4^{+}$ T cells, immunosuppressive Treg cells, and pro-inflammatory Th17 cells in mice treated with mock EVs, RVG-HA, or RVG-EVs compared to those treated with PBS ($n = 6$ for each group). Data were analysed using one-way ANOVA followed by the Holm-Sidak post hoc multiple comparison test

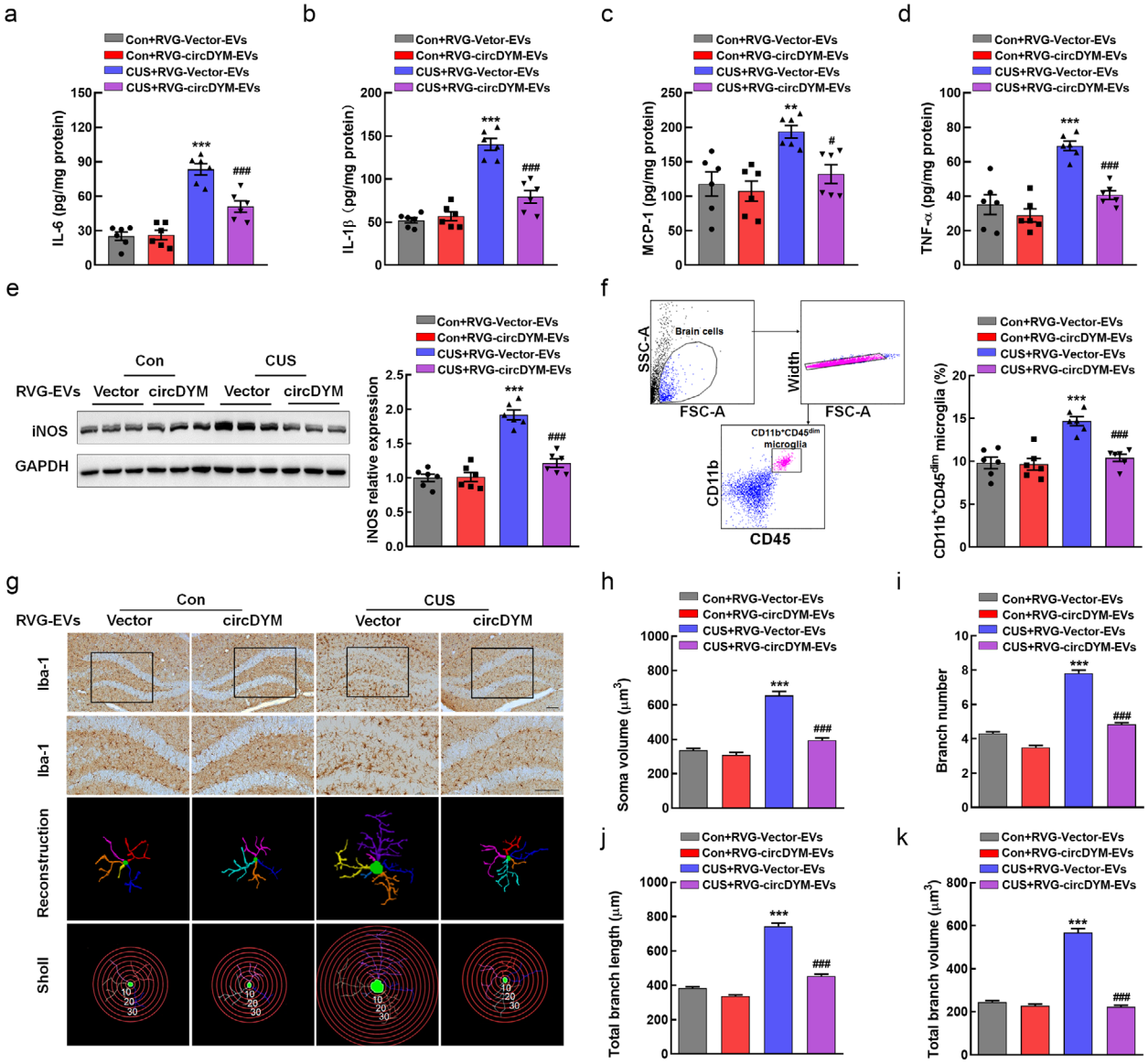

FIGURE 7 RVG-EV-mediated delivery of circDYM attenuated microglial activation. (a–d) Level of IL-6 (a), IL-1β (b), MCP-1 (c), and TNF-α (d) measured by ELISA in the hippocampus after RVG-circDYM-EVs administration with or without CUS treatment ($n = 6$ for each group). $^{**}P < 0.01$, $^{***}P < 0.001$ versus the Control + RVG-Vector-EVs group; $^{\#}P < 0.05$, $^{\#\#\#}P < 0.001$ versus the CUS + RVG-Vector-EVs group using two-way ANOVA followed by the Holm-Sidak post hoc multiple comparison test. (e) Representative western blots of iNOS levels after RVG-circDYM-EVs administration with or without CUS treatment ($n = 6$ for each group). $^{***}P < 0.001$ versus the Control + RVG-Vector-EVs group; $^{\#\#\#}P < 0.001$ versus the CUS + RVG-Vector-EVs group using two-way ANOVA followed by the Holm-Sidak post hoc multiple comparison test. (f) FCM analysis of $CD11b^{+}CD45^{dim}$ microglial cells isolated from the CUS mouse brain by the Percoll gradient method ($n = 6$ for each group). $^{***}P < 0.001$ versus the Control + RVG-Vector-EVs group; $^{\#\#\#}P < 0.001$ versus the CUS + RVG-Vector-EVs group using two-way ANOVA followed by the Holm-Sidak post hoc multiple comparison test. (g–k) RVG-circDYM-EVs inhibited microglial activation in the CUS mouse hippocampus. Representative images of microglial immunostaining for Iba-1, followed by 3D reconstruction and Sholl analysis (g). Scale bar: 50 μm. Average soma volume (h), branch number (i), total branch length (j), and total branch volume (k). ($n = 6$ mice for each group, 60 cells for each group). $^{***}P < 0.001$ versus the Control + RVG-Vector-EVs group; $^{\#\#\#}P < 0.001$ versus the CUS + RVG-Vector-EVs group using two-way ANOVA followed by the Holm-Sidak post hoc multiple comparison test. ELISA, Enzyme-linked immunosorbent assay; SSC-A, side scatter area; FSC-A, forward scatter area. Images of unedited full blots in Figure S18

these results suggested that RVG-circDYM-EVs enhanced BBB integrity and inhibited the infiltration of peripheral immune cells, including lymphocytes and myeloid cells, into the brain of CUS mice.

3.9 | CircDYM directly bound to TAF1 to regulate microglial activation

To identify the molecular mechanisms involved in the neuroinflammation, transcriptome analysis was performed in circDYM-overexpressing primary mouse microglia. As shown in Figure 8a, a total of 59 genes were differentially sifted with cutoffs of

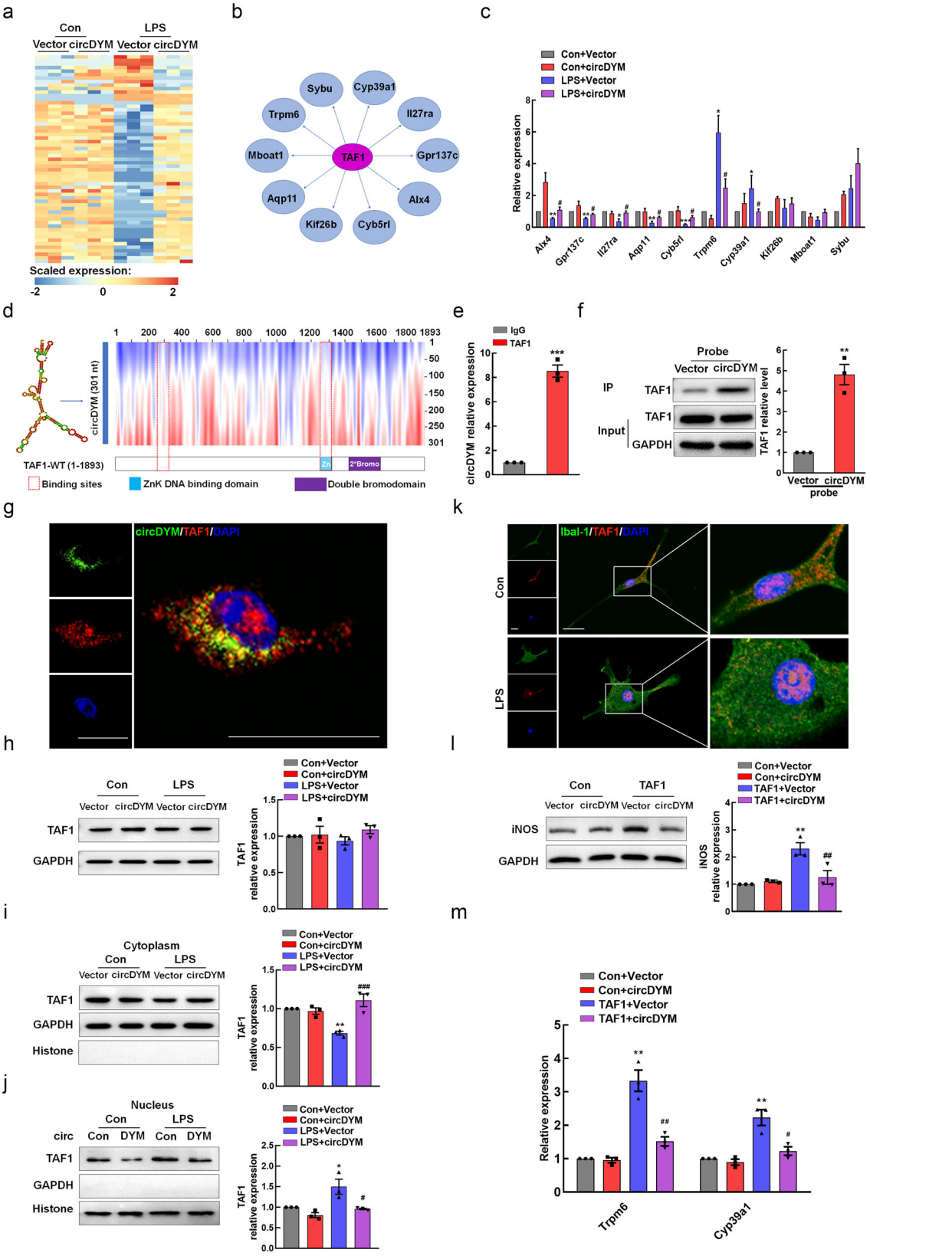

FIGURE 8 CircDYM directly bound to TAF1 to regulate microglial activation. (a) Microarray heat map assessing the variation in mRNA expression in primary mouse microglia with overexpressed circDYM and vector treated with or without LPS. ($n = 3$ for each group) (b) Prediction of transcriptor-mRNA interaction using the GTRD algorithm. (c) qPCR analysis of the expression of potential TAF1 target genes in LPS-induced primary mouse microglia after circDYM overexpression. All data were presented as mean ± SEM of three independent experiments. $^{*}P < 0.05$, $^{**}P < 0.01$, $^{***}P < 0.001$ versus the Control + Vector group; $^{\#}P < 0.05$ versus the LPS + Vector group using two-way repeated measures ANOVA followed by the Holm-Sidak post hoc multiple comparison test. (d) Prediction of circDYM-TAF1 interaction using the catPAPID algorithm and schematic of TAF1 with functional protein domains. (e) qPCR analysis of

[$\log_2$(fold change)] ≥ 1 and adjusted *P*-value < 0.05. Because circRNA have protein-binding capacities, TRCirc (a database on circRNA transcription regulation) was used to identify proteins that interact with circDYM. Combined with GTRD-a database on gene transcription regulation, we identified that TAF1 potentially regulated 10 differentially expressed (DE) genes (Figure 8b). Next, we verified the expression of the 10 DE genes by qPCR and found that seven of them have the same trends in RNA sequencing results (Figure 8c). Then, the catRAPID algorithm was use to predict that circDYM binds strongly to TAF1. Two TAF1-amino acid locations (277-322 and 1256–1303) presented high interaction capacity with circDYM (Figure 8d). RIP assay verified the strong affinity between circDYM and TAF1 (Figure 8e). Meanwhile, RNA pull-down assay conducted with the biotinylated circDYM probe showed that the circDYM probe pulled down higher levels of TAF1 than the circControl probe (Figure 8f). In addition, FISH analysis visually showed that circDYM and TAF1 co-localized in the cytoplasm of primary mouse microglia (Figure 8g).

To verify whether the interaction of circDYM and TAF1 affects the expression and distribution of TAF1, western blot was performed to examine the total expression of TAF1 on primary mouse microglial cells in the presence of LPS, which showed no significant difference between LPS + circDYM and LPS + circControl groups (Figure 8h). Interestingly, circDYM increased the TAF1 level in the cytoplasms and decreased its level in the nuclei of microglial cells in the presence of LPS (Figure 8i–j). Subsequent immunofluorescence staining confirmed this finding (Figure 8k). Subcellular distribution changes of TAF1 were also demonstrated in the hippocampus tissues of CUS mice treated with RVG-circDYM-EVs (Figure S13a–c). To further confirm that TAF1 is a mediator of circDYM, circDYM-GFP lentivirus and TAF1 overexpressed plasmid were co-transfected into primary mouse microglial cells. Overexpression of circDYM attenuated the effect of TAF1 on microglial activation, as indicated by the expression of iNOS levels (Figure 8l).

To dissect whether TAF1 mediated the expression of these target genes, circDYM-GFP lentivirus and TAF1 overexpressed plasmid were co-transfected into primary mouse microglial cells. As shown in Figure 8m, overexpression of TAF1 significantly increased the expression of *Trpm6* and *Cyp39a1* mRNA, which were inhibited by the overexpression of circDYM. As predicted by combination of GTRD and ALGGEN (Algorithmics and Genetics Group), putative TAF1 binding sites were found within the promoter regions of *Trpm6* and *Cyp39a1*. Moreover, LPS treatment increased the binding of TAF1 to the promoters of *Trpm6* and *Cyp39a1* (Figure S14). To verify that TRPM6 and CYP39A1 modulate the expression of iNOS, primary mouse microglia were transfected with *Trpm6* siRNA (siRNA-Trpm6) or *Cyp39a1* siRNA (siRNA-Cyp39a1). As shown in Figure S15a,b, knockdown of *Trpm6* efficiently decreased *Trpm6* expression and significantly reversed LPS-induced increase of iNOS. Similarly, knockdown of *Cyp39a1* had the same effect (Figure S15c,d). Together, these results demonstrated that TAF1 could regulate microglial activation by its downstream target genes *Trpm6* and *Cyp39a1*.

4 | DISCUSSION

In this study, we successfully performed targeted delivery of circDYM to the brain via engineered RVG-EVs and demonstrated that RVG-circDYM-EVs significantly ameliorated depressive-like behaviours in CUS mouse models with remission of microglial activation, astrocyte dysfunction, BBB leakiness, and peripheral immune cell infiltration. Functional study revealed that circDYM binds with transcription factor TAF1 to downregulate its downstream target genes *Trpm6* and *Cyp39a1* (Figure 9).

Currently, the development of drugs for the treatment of MDD is limited by the complex challenges that are posed by the neurovascular unit. One of the main obstacles is the presence of the BBB, which tightly controls entry of molecules and cells into the brain, restricting the delivery of therapeutics (Abbott et al., 2010). Conventional approaches that use the drug molecules in their free form have demonstrated poor BBB penetration due to the presence of efflux pumps on the endothelial cells that strictly regulate the movement of drug molecules (De Bock et al., 2016; Samal et al., 2019). EVs recently have been employed to

relative enrichment of endogenous circDYM in TAF1 RIP. All data were presented as mean ± SEM of three independent experiments. $^{***}P < 0.001$ versus the IgG group using Student's *t*-test. (f) Western blot analysis of relative enrichment of endogenous TAF1 in circDYM RIP. All data were presented as mean ± SEM of three independent experiments. $^{**}P < 0.01$ versus the Vector group using Student's *t*-test. (g) Co-localization of circDYM and TAF1 in the cytoplasm of primary mouse microglia by FISH analysis. Green: circDYM; Red: TAF1; Blue: DAPI. Scale bar: 20 μm. (h–j) Western blot analysis of TAF1 protein levels (h) and cytoplasmic (i) or nuclear (j) localization of TAF1 in primary mouse microglia after vector or circDYM lentivirus transduction with or without treated with LPS (100 ng ml^{-1}) for 24 h. The purity of cell subcellular fractions was assessed by western blotting against specific markers. All data were presented as mean ± SEM of three independent experiments. $^{*}P < 0.05$, $^{**}P < 0.01$ versus the Control + Vector group; $^{\#}P < 0.05$, $^{\#\#\#}P < 0.001$ versus the LPS + Vector group using two-way ANOVA followed by the Holm-Sidak post hoc multiple comparison test. (k) Distribution of TAF1 in primary microglia. Primary mouse microglia were subjected to immunocytochemistry analysis of TAF1 and Iba-1 proteins and DAPI staining of genomic DNA with or without LPS treatment. Scale bar: 20 μm. (l) Overexpression of circDYM significantly inhibited iNOS expression induced by TAF1 in primary mouse microglia. All data were presented as mean ± SEM of three independent experiments. $^{**}P < 0.01$ versus the Control + Vector group; $^{\#\#}P < 0.01$ versus the TAF1 +Vector group using two-way repeated measures ANOVA followed by the Holm-Sidak post hoc multiple comparison test. (m) qPCR analysis of the expression of potential TAF1 target genes in primary mouse microglia after overexpression of circDYM or TAF1. All data were presented as mean ± SEM of three independent experiments. $^{**}P < 0.01$ versus the Control + Vector group; $^{\#}P < 0.05$, $^{\#\#}P < 0.01$ versus the TAF1 +Vector group using two-way repeated measures ANOVA followed by the Holm-Sidak post hoc multiple comparison test. Images of unedited full blots in Figure S19

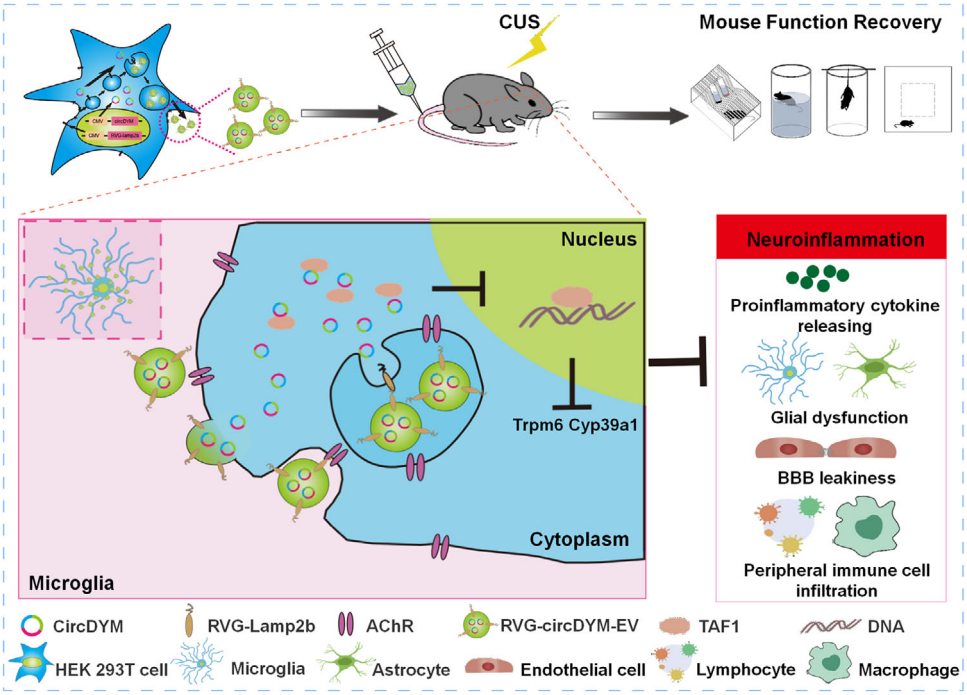

FIGURE 9 Schematic illustration of the effect of RVG-circDYM-EVs on the functional recovery in CUS mice. Intravenous administration of RVG-circDYM-EVs following CUS treatment significantly ameliorated depressive-like behaviours by inhibiting neuroinflammation. CircDYM binds to TAF1 and downregulates multiple downstream genes (*Trpm6*, *Cyp39a1*) to maintain brain functions

deliver exogenous nucleic acid drugs to specific cell types or tissues in vivo due to their multiple versatility, low immunogenicity, and ability to pass through the BBB (Kojima et al., 2018; Yong et al., 2019). However, the intravenous delivery of EVs into the brain remains a challenge due to poor targeting of unmodified EVs (Smyth et al., 2015). In our study, RVG-EVs successfully incorporated circDYM improved drug targeting brain compared with the unmodified-EV-encapsulated circDYM, suggesting that RVG-circDYM-EVs might be taken as a potential delivery system for MDD treatment (Alvarez-Erviti et al., 2011; Hung & Leonard, 2015).

Fluorescent lipophilic membrane dyes have certain limitations, such as lipid staining of non-EV species, similarity in size and fluorescence intensity with EVs, and desorption from EVs into blood (Münter et al., 2018; Pužar Dominkuš et al., 2018; Shimomura et al., 2021; Simonsen, 2019; Takov et al., 2017), all of which pose challenges for EV tracking. Based on previous studies (Karimi et al., 2018; Pužar Dominkuš et al., 2018), a combination of ultracentrifugation, density cushion separation, and spatial exclusion chromatography (SEC) was performed to isolate and purify Dil or DiR-labelled EVs in this study. We observed that the entry of Dil-labelled RVG-EVs into the brain was significantly higher than that of mock EVs with the same dose. The co-localization of the lake blue signal of HA (Tag-stabilized peptide-RVG fusion protein) and the red signal of Dil was observed in the hippocampus of mice after RVG-EV injection, while there were no co-localization signals for mock EVs. These findings suggest that the isolated and purified Dil or DiR-labelled EVs are reliable for tracking EVs in vivo. Other EV labelling methods provide a more specific way of tracking EVs, such as using an encoded fluorescent reporter (CD63-eGFP) or a cytoplasmic dye (Sutaria et al., 2017; Van Der Vlist et al., 2012). However, these methods have low efficiency in transfection or adverse effects on immune cell function. Our experimental design was applied to minimize these issues related to fluorescent lipophilic membrane dyes.

Although modification of EVs with RVG enhanced brain targeting, consistent with previous study (Imai et al., 2015; Wiklander et al., 2015), we observed significantly enrichment of EVs in peripheral organs, particularly in the liver. Meanwhile, we also observed that the expression of circDYM in the liver was highest among all organs within 6 h after RVG-circDYM-EVs injection, while decreased sharply over time. Mounting studies have indicated that macrophages in mononuclear phagocyte system (MPS) is involved in the uptake and clearance of EVs intravenously injected from the systemic circulation (Imai et al., 2015; Wan et al., 2020). Consistent with those studies, our study suggested that circDYM delivered by RVG-EVs were preferentially accumulated in the liver, mainly due to the presence of MPS, and then quickly degraded by macrophages.

Therapeutically, administration of RVG-circDYM-EVs relieved depressive-like behaviours in CUS mice. Furthermore, circDYM delivered by RVG-EVs significantly reduced CNS inflammation by inhibition of microglial activation, in addition to remission of astrocyte dysfunction, BBB leakiness and peripheral immune cell infiltration. Chronic stress has been indicated to induce depressive-like behaviours in mice by promotion of CNS inflammation (Fan et al., 2018; Song et al., 2020). Microglia

function as the primary regulators of inflammatory responses and their activation can evoke the production of various mediators, including iNOS, proinflammatory cytokines to contribute to CNS inflammation (Gopinath et al., 2020; Jia et al., 2018). Consist with previous studies (70, Franklin et al., 2018), the current study demonstrated that circDYM delivered by RVG-EVs alleviated CUS-induced depressive-like behaviours by inhibition of microglial activation.

Increasing evidence indicates that circRNAs have different biological functions (Thomson & Dinger, 2016). Our previous study demonstrated that the restoration of circDYM attenuated depressive-like behaviours by targeting miR-9 to regulate microglial activation via HSP90 ubiquitination (Zhang et al., 2020). Besides the function of "miRNA-sponge", mounting studies have demonstrated that circRNAs can bind with RNA-binding proteins and affect their distribution and function (Huang, He et al., 2019, Huang, Li et al., 2019). In the present study, we found that circDYM relieved depressive-like behaviours by binding with the transcription activator-TAF1, resulting in the inhibition of TAF1 in the nucleus and a decreased expression of downstream molecules including TRPM6 and CYP39A1. Thus, circDYM appears to have multi-target effects, indicating it a promising therapeutic candidate for treating MDD.

Bioinformatic prediction, RNA RIP, pull-down and FISH assays were performed to confirm the interaction between TAF1 and circDYM. TAF1 is a key component of the transcription factor IID complex that plays an important role in transcription initiation (Louder et al., 2016), which is involved in the cell cycle and proliferation (Gudmundsson et al., 2019; Xu et al., 2019). Previous studies have reported that TAF1 mutations are linked to severe neurodevelopmental defects (Hernández et al., 2020), and the absence of TAF1 is associated with glial dysfunction (Janakiraman et al., 2020). Our results suggest that TAF1 regulates microglial activation and its activity is regulated by circDYM.

In the present study, circDYM/TAF1 regulated microglial activation through TRPM6 and CYP39A1. Computational algorithms such as ALGGEN have been employed to identify TAF1 binding sites located within the promoter of *Trpm6* and *Cyp39a1*. Consistent with these predictions, the present study indicated that TAF1 directly regulate *Trpm6* and *Cyp39a1* expression based on ChIP assays. Transient receptor potential melastatin 6 (TRPM6) is a magnesium channel and involved in the cellular magnesium homeostasis (Lima & Fock, 2020). TRPM6 has recently been discovered in immune cells and upregulated under oxidative stress in human monocytes (Wuensch et al., 2010). Moreover, knockdown of TRPM6 alleviated oxidative stress and inflammatory response by activation of the TGF-β/Smads signalling pathway (Wu et al., 2019). These studies indicate that TRPM6 may play a role in the inflammatory process. Cytochrome P450 enzymes 39A1 (CYP39A1), which is an oxysterol metabolizing enzyme, regulates cholesterol and oxysterols homeostasis (Grabovec et al., 2019). In a previous study, *Cyp39a1* was found to be elevated in mice brain with western diet-induced systemic inflammation (Jena et al., 2018). Consist with these findings, we demonstrated that circDYM decreased the levels of *Trpm6* and *Cyp39a1* in microglial cells in the presence of LPS. Furthermore, knockdown of *Trpm6* and *Cyp39a1* significantly reversed LPS-induced increase of iNOS.

Ongoing EV-based clinical trials aim to identify diagnostic or prognostic biomarkers, and utilize EVs as drugs for treatment of various diseases, while EVs as drugs carriers for delivery of gene therapy agents have been explored, to date no clinical trials based on these technologies have been reported (Athauda et al., 2019; Krug et al., 2018; Mckiernan et al., 2018; Perocheau et al., 2021). Although it makes great progress on EVs-based drug delivery system, it should be pointed out that there exit many challenges in a clear understanding of EVs regarding therapeutic cargo loading and assembly for drug delivery. Obstacles such as no distinct ideal purification technique for isolation and separation of EVs with high purity, limit clinical application of EV-based drug delivery (Schulz-Siegmund & Aigner, 2021). Novel and improved manufacturing strategies initially developed in academic settings need to be adapted for scaling up to meet adequate manufacturing practice requirements. In addition, to achieve targeting ability of EVs, ligands are attached to the surface through chemical conjugation and these active targeting molecular combinational techniques and systems need to be examined for safety and efficacy. Nevertheless, utilizing and expanding on this opportunity to overcome challenges in delivering therapy to the brain, in the future could lead to safe and efficient production of EVs. Taken together, the present study indicated that RVG-EVs enhanced the efficiency of circDYM delivery, suggesting that EV-based circDYM delivery is a promising therapeutic strategy for treatment of MDD.

ACKNOWLEDGEMENTS

This work was supported by grants from the National Natural Science Foundation of Distinguished Young Scholars (82025033), the National Key Research and Development Program of China (Grant No. 2021ZD0202900, 2017YFA0104303), the National Natural Science Foundation of China (Grant Nos. 81761138048, 81673410 and 81973304), the CAMS Innovation Fund for Medical Sciences (CIFMS) (Grant No. 2016-I2M-1-004), the Natural Science Foundation of Jiangsu Province (Grant No. BK20191265), National Science and Technology Major Project (Grant No. 2020 ZX09201015), Fundamental Research Funds for the Central Universities (Grant No. 2242021R41098), the National Natural Science Foundation of China (Grant No. BK2020358), the National Natural Science Foundation of China (Grant No. 82003733), and the Jiangsu Innovation and Entrepreneurship Team Program.

CONFLICT OF INTEREST

The author declared no conflict of interest.

REFERENCES

Abbott, N. J., Patabendige, A. A. K., Dolman, D. E. M., Yusof, S. R., & Begley, D. J. (2010). Structure and function of the blood-brain barrier. *Neurobiology of Disease*, *37*, 13–25.

Alvarez-Erviti, L., Seow, Y., Yin, H., Betts, C., Lakhal, S., & Wood, M. J. A. (2011). Delivery of siRNA to the mouse brain by systemic injection of targeted exosomes. *Nature Biotechnology*, *29*, 341–345.

Arnow, B. A., Blasey, C., Williams, L. M., Palmer, D. M., Rekshan, W., Schatzberg, A. F., Etkin, A., Kulkarni, J., Luther, J. F., & Rush, A. J. (2015). Depression subtypes in predicting antidepressant response: A report from the iSPOT-D trial. *American Journal of Psychiatry*, *172*, 743–750.

Athauda, D., Gulyani, S., Karnati, H. K., Li, Y., Tweedie, D., Mustapic, M., Chawla, S., Chowdhury, K., Skene, S. S., Greig, N. H., Kapogiannis, D., & Foltynie, T. (2019). Utility of neuronal-derived exosomes to examine molecular mechanisms that affect motor function in patients with Parkinson disease: A secondary analysis of the exenatide-PD trial. *JAMA Neurology*, *76*, 420–429.

Belzeaux, R., Gorgievski, V., Fiori, L. M., Lopez, J. P., Grenier, J., Lin, R., Nagy, C., Ibrahim, ElC, Gascon, E., Courtet, P., Richard-Devantoy, S., Berlim, M., Chachamovich, E., Théroux, J. -F., Dumas, S., Giros, B., Rotzinger, S., Soares, C. N., Foster, J. A., …Turecki, G. (2020). GPR56/ADGRG1 is associated with response to antidepressant treatment. *Nature Communication*, *11*, 1635.

Berda-Haddad, Y., Robert, S., Salers, P., Zekraoui, L., Farnarier, C., Dinarello, C. A., Dignat-George, F., & Kaplanski, G. (2011). Sterile inflammation of endothelial cell-derived apoptotic bodies is mediated by interleukin-1alpha. *PNAS*, *108*, 20684–20689.

Cao, X., Li, L. -P., Wang, Q., Wu, Q., Hu, H. -H., Zhang, M., Fang, Y. -Y., Zhang, J., Li, S-Ji, Xiong, W. -C., Yan, H. -C., Gao, Yu-Bo, Liu, Ji-H, Li, X. -W., Sun, Li-R, Zeng, Y. -N., Zhu, X. -H., & Gao, T. -M. (2013). Astrocyte-derived ATP modulates depressive-like behaviors. *Nature Medicine*, *19*, 773–777.

Charlson, F., Van Ommeren, M., Flaxman, A., Cornett, J., Whiteford, H., & Saxena, S. (2019). New WHO prevalence estimates of mental disorders in conflict settings: a systematic review and meta-analysis. *Lancet*, *394*, 240–248.

Chen, Ri-X, Chen, X., Xia, L. -P., Zhang, J. -X., Pan, Z. -Z., Ma, X. -D., Han, K., Chen, J. -W., Judde, J. -G., Deas, O., Wang, F., Ma, N. -F., Guan, X., Yun, J. -P., Wang, F. -W., Xu, R. -H., & Dan Xie, (2019). N(6)-methyladenosine modification of circNSUN2 facilitates cytoplasmic export and stabilizes HMGA2 to promote colorectal liver metastasis. *Nature Communication*, *10*, 4695.

Chivero, E. T., Liao, Ke, Niu, F., Tripathi, A., Tian, C., Buch, S., & Hu, G. (2020). Engineered extracellular vesicles loaded with miR-124 attenuate cocaine-mediated activation of microglia. *Frontiers in Cell and Developmental Biology*, *8*, 573.

Cui, X., Niu, W., Kong, L., He, M., Jiang, K., Chen, S., Zhong, A., Li, W., Lu, J., & Zhang, L. (2016). hsa_circRNA_103636: Potential novel diagnostic and therapeutic biomarker in Major depressive disorder. *Biomarkers in Medicine*, *10*, 943–952.

Davey, C. G., Chanen, A. M., Hetrick, S. E., Cotton, S. M., Ratheesh, A., Amminger, G. P., Koutsogiannis, J., Phelan, M., Mullen, E., Harrison, B. J., Rice, S., Parker, A. G., Dean, O. M., Weller, A., Kerr, M., Quinn, A. L., Catania, L., Kazantzis, N., Mcgorry, P. D., & Berk, M. (2019). The addition of fluoxetine to cognitive behavioural therapy for youth depression (YoDA-C): A randomised, double-blind, placebo-controlled, multicentre clinical trial. *Lancet Psychiatry*, *6*, 735–744.

De Bock, M., Van Haver, V., Vandenbroucke, R. E., Decrock, E., Wang, N., & Leybaert, L. (2016). Into rather unexplored terrain-transcellular transport across the blood-brain barrier. *Glia*, *64*, 1097–1123.

Elashiry, M., Elashiry, M. M., Elsayed, R., Rajendran, M., Auersvald, C., Zeitoun, R., Rashid, M. H., Ara, R., Meghil, M. M., Liu, Y., Arbab, A. S., Arce, R. M., Hamrick, M., Elsalanty, M., Brendan, M., Pacholczyk, R., & Cutler, C. W. (2020). Dendritic cell derived exosomes loaded with immunoregulatory cargo reprogram local immune responses and inhibit degenerative bone disease in vivo. *Journal of Extracellular Vesicles*, *9*, 1795362.

El-Hage, W., Leman, S., Camus, V., & Belzung, C. (2013). Mechanisms of antidepressant resistance. *Frontires in Pharmacology*, *4*, 146.

Fan, C., Song, Q., Wang, P., Li, Ye, Yang, Mu, Liu, B., & Yu, S. Y. (2018). Curcumin protects against chronic stress-induced dysregulation of neuroplasticity and depression-like behaviours via suppressing IL-1beta pathway in rats. *Neuroscience*, *392*, 92–106.

Firk, C., & Markus, C. R. (2007). Review: Serotonin by stress interaction: a susceptibility factor for the development of depression? *Journal of Psychopharmacology*, *21*, 538–544.

Franklin, T. C., Wohleb, E. S., Zhang, Yi, Fogaça, M., Hare, B., & Duman, R. S. (2018). Persistent increase in microglial RAGE contributes to chronic stress-induced priming of depressive-like behaviour. *Biological Psychiatry*, *83*, 50–60.

Gopinath, A., Collins, A., Khoshbouei, H., & Streit, W. J. (2020). Microglia and other myeloid cells in CNS health and disease. *Journal of Pharmacology and Experimental Therapeutics*.

Grabovec, I. P., Smolskaya, S. V., Baranovsky, A. V., Zhabinskii, V. N., Dichenko, Y. V., Shabunya, P. S., Usanov, S. A., & Strushkevich, N. V. (2019). Ligand-binding properties and catalytic activity of the purified human 24-hydroxycholesterol 7alpha-hydroxylase, CYP39A1. *Journal of Steroid Biochemistry and Molecular Biology*, *193*, 105416.

Gudmundsson, S., Wilbe, M., Filipek-Górniok, B., Molin, A. -M., Ekvall, S., Johansson, J., Allalou, A., Gylje, H., Kalscheuer, V. M., Ledin, J., Annerén, G., & Bondeson, M. -L. (2019). TAF1, associated with intellectual disability in humans, is essential for embryogenesis and regulates neurodevelopmental processes in zebrafish. *Science Reports*, *9*, 10730.

Hacein-Bey-Abina, S., Garrigue, A., Wang, G. P., Soulier, J., Lim, A., Morillon, E., Clappier, E., Caccavelli, L., Delabesse, E., Beldjord, K., Asnafi, V., Macintyre, E., Dal Cortivo, L., Radford, I., Brousse, N., Sigaux, F., Moshous, D., Hauer, J., Borkhardt, A., … Cavazzana-Calvo, M. (2008). Insertional oncogenesis in 4 patients after retrovirus-mediated gene therapy of SCID-X1. *Journal of Clinical Investigation*, *118*, 3132–3142.

Hacein-Bey-Abina, S., Von Kalle, C., Schmidt, M., Mccormack, M. P., Wulffraat, N., Leboulch, P., Lim, A., Osborne, C. S., Pawliuk, R., Morillon, E., Sorensen, R., Forster, A., Fraser, P., Cohen, J. I., De Saint Basile, G., Alexander, I., Wintergerst, U., Frebourg, T., Aurias, A., … Cavazzana-Calvo, M. (2003). LMO2-associated clonal T cell proliferation in two patients after gene therapy for SCID-X1. *Science*, *302*, 415–419.

Hernández, I. H., Cabrera, J. R., Santos-Galindo, M., Sánchez-Martín, M., Domínguez, V., García-Escudero, R., Pérez-Álvarez, M. J., Pintado, B., & Lucas, J. J. (2020). Pathogenic SREK1 decrease in Huntington's disease lowers TAF1 mimicking X-linked dystonia parkinsonism. *Brain*, *143*, 2207–2219.

Huang, R., Zhang, Y., Bai, Y., Han, B., Ju, M., Chen, B., Yang, Li, Wang, Yu, Zhang, H., Zhang, H., Xie, C., Zhang, Z., & Yao, H. (2020). N(6)-methyladenosine modification of fatty acid amide hydrolase messenger RNA in circular RNA STAG1-regulated astrocyte dysfunction and depressive-like behaviours. *Biological Psychiatry*, *88*, 392–404.

Huang, S., Li, X., Zheng, H., Si, X., Li, B., Wei, G., Li, C., Chen, Y., Chen, Y., Liao, W., Liao, Y., & Bin, J. (2019). Loss of super-enhancer-regulated circRNA Nfix induces cardiac regeneration after myocardial infarction in adult mice. *Circulation*, *139*, 2857–2876.

Huang, X., He, M., Huang, S., Lin, R., Zhan, M., Yang, D., Shen, H., Xu, S., Cheng, W., Yu, J., Qiu, Z., & Wang, J. (2019). Circular RNA circERBB2 promotes gallbladder cancer progression by regulating PA2G4-dependent rDNA transcription. *Molecular Cancer*, *18*, 166.

Hung, M. E., & Leonard, J. N. (2015). Stabilization of exosome-targeting peptides via engineered glycosylation. *Journal of Biological Chemistry*, *290*, 8166–8172.

Imai, T., Takahashi, Y., Nishikawa, M., Kato, K., Morishita, M., Yamashita, T., Matsumoto, A., Charoenviriyakul, C., & Takakura, Y. (2015). Macrophage-dependent clearance of systemically administered B16BL6-derived exosomes from the blood circulation in mice. *Journal of Extracellular Vesicles*, *4*, 26238.

Janakiraman, U., Dhanalakshmi, C., Yu, J., Moutal, A., Boinon, L., Fukunaga, K., Khanna, R., & Nelson, M. A. (2020). The investigation of the T-type calcium channel enhancer SAK3 in an animal model of TAF1 intellectual disability syndrome. *Neurobiology of Disease*, *143*, 105006.

Jena, P. K., Sheng, L., Di Lucente, J., Jin, L. -. W., Maezawa, I., & Wan, Y. -J. Y. (2018). Dysregulated bile acid synthesis and dysbiosis are implicated in Western diet-induced systemic inflammation, microglial activation, and reduced neuroplasticity. *FASEB Journal*, *32*, 2866–2877.

Jia, X., Gao, Z., & Hu, H. (2018). Microglia in depression: Current perspectives. *Science China Life Science*.

Karimi, N., Cvjetkovic, A., Jang, SuC, Crescitelli, R., Hosseinpour Feizi, M. A., Nieuwland, R., Lötvall, J., & Lässer, C. (2018). Detailed analysis of the plasma extracellular vesicle proteome after separation from lipoproteins. *Cellular and Molecular Life Sciences*, *75*, 2873–2886.

Katz, R. J., & Sibel, M. (1982). Further analysis of the specificity of a novel animal model of depression—Effects of an antihistaminic, antipsychotic and anxiolytic compound. *Pharmacology Biochemistry and Behaviour*, *16*, 979–982.

Kendler, K. S., Kuhn, J. W., & Prescott, C. A. (2004). Childhood sexual abuse, stressful life events and risk for major depression in women. *Psychological Medicine*, *34*, 1475–1482.

Kim, S. -S., Ye, C., Kumar, P., Chiu, I., Subramanya, S., Wu, H., Shankar, P., & Manjunath, N. (2010). Targeted delivery of siRNA to macrophages for anti-inflammatory treatment. *Molecular Therapy*, *18*, 993–1001.

Kojima, R., Bojar, D., Rizzi, G., Hamri, G. C., El-Baba, M. D., Saxena, P., Ausländer, S., Tan, K. R., & Fussenegger, M. (2018). Designer exosomes produced by implanted cells intracerebrally deliver therapeutic cargo for Parkinson's disease treatment. *Nature Communication*, *9*, 1305.

Kristensen, L. S., Andersen, M. S., Stagsted, L. V. W., Ebbesen, K. K., Hansen, T. B., & Kjems, J. (2019). The biogenesis, biology and characterization of circular RNAs. *Nature Reviews Genetics*, *20*, 675–691.

Krug, A. K., Enderle, D., Karlovich, C., Priewasser, T., Bentink, S., Spiel, A., Brinkmann, K., Emenegger, J., Grimm, D. G., Castellanos-Rizaldos, E., Goldman, J. W., Sequist, L. V., Soria, J. -C., Camidge, D. R., Gadgeel, S. M., Wakelee, H. A., Raponi, M., Noerholm, M., & Skog, J. (2018). Improved EGFR mutation detection using combined exosomal RNA and circulating tumor DNA in NSCLC patient plasma. *Annals of Oncology*, *29*, 700–706.

Lener, T., Gimona, M., Aigner, L., Börger, V., Buzas, E., Camussi, G., Chaput, N., Chatterjee, D., Court, F. A., Portillo, H. A. D., O'driscoll, L., Fais, S., Falcon-Perez, J. M., Felderhoff-Mueser, U., Fraile, L., Gho, Y. S., Görgens, A., Gupta, R. C., Hendrix, A., … Giebel, B. (2015). Applying extracellular vesicles based therapeutics in clinical trials—An ISEV position paper. *Journal of Extracellular Vesicles*, *4*, 30087.

Lima, F. D. S., & Fock, R. A. (2020). A review of the action of magnesium on several processes involved in the modulation of hematopoiesis. *International Journal of Molecular Sciences*, *21*, 7084.

Lin, Y., Zhang, C., Xiang, P., Shen, J., Sun, W., & Yu, H. (2020). Exosomes derived from HeLa cells break down vascular integrity by triggering endoplasmic reticulum stress in endothelial cells. *Journal of Extracellular Vesicles*, *9*, 1722385.

Liu, C. -X., Li, X., Nan, F., Jiang, S., Gao, X., Guo, Si-K, Xue, W., Cui, Y., Dong, K., Ding, H., Qu, Bo, Zhou, Z., Shen, N., Yang, Li, & Chen, L. -L. (2019). Structure and degradation of circular RNAs regulate PKR activation in innate immunity. *Cell*, *177*, 865–880.e21 e821.

Louder, R. K., He, Y., López-Blanco, J. R., Fang, J., Chacón, P., & Nogales, E. (2016). Structure of promoter-bound TFIID and model of human pre-initiation complex assembly. *Nature*, *531*, 604–609.

Malhi, G. S., & Mann, J. J. (2018). Depression. *Lancet*, *392*, 2299–2312.

Matcovitch-Natan, O., Winter, D. R., Giladi, A., Vargas Aguilar, S., Spinrad, A., Sarrazin, S., Ben-Yehuda, H., David, E., Zelada González, F., Perrin, P., Keren-Shaul, H., Gury, M., Lara-Astaiso, D., Thaiss, C. A., Cohen, M., Bahar Halpern, K., Baruch, K., Deczkowska, A., Lorenzo-Vivas, E., …Amit, I. (2016). Microglia development follows a stepwise program to regulate brain homeostasis. *Science*, *353*, aad8670.

Mckiernan, J., Donovan, M. J., Margolis, E., Partin, A., Carter, B., Brown, G., Torkler, P., Noerholm, M., Skog, J., Shore, N., Andriole, G., Thompson, I., & Carroll, P. (2018). A prospective adaptive utility trial to validate performance of a novel urine exosome gene expression assay to predict high-grade prostate cancer in patients with prostate-specific antigen 2-10 ng/ml at initial biopsy. *European Urology*, *74*, 731–738.

Meltzer-Brody, S., Colquhoun, H., Riesenberg, R., Epperson, C. N., Deligiannidis, K. M., Rubinow, D. R., Li, H., Sankoh, A. J., Clemson, C., Schacterle, A., Jonas, J., & Kanes, S. (2018). Brexanolone injection in post-partum depression: Two multicentre, double-blind, randomised, placebo-controlled, phase 3 trials. *Lancet*, *392*, 1058–1070.

Menard, C., Pfau, M. L., Hodes, G. E., Kana, V., Wang, V. X., Bouchard, S., Takahashi, A., Flanigan, M. E., Aleyasin, H., Leclair, K. B., Janssen, W. G., Labonté, B., Parise, E. M., Lorsch, Z. S., Golden, S. A., Heshmati, M., Tamminga, C., Turecki, G., Campbell, M., …Russo, S. J. (2017). Social stress induces neurovascular pathology promoting depression. *Nature Neuroscience*, *20*, 1752–1760.

Miller, A. H., & Raison, C. L. (2016). The role of inflammation in depression: From evolutionary imperative to modern treatment target. *Nature Reviews Immunology*, *16*, 22–34.

Münter, R., Kristensen, K., Pedersbæk, D., Larsen, J. B., Simonsen, J. B., & Andresen, T. L. (2018). Dissociation of fluorescently labeled lipids from liposomes in biological environments challenges the interpretation of uptake studies. *Nanoscale*, *10*, 22720–22724.

Murrough, J. W., Abdallah, C. G., & Mathew, S. J. (2017). Targeting glutamate signalling in depression: progress and prospects. *Nature Reviews Drug Discovery*, *16*, 472–486.

Perocheau, D., Touramanidou, L., Gurung, S., Gissen, P., & Baruteau, J. (2021). Clinical applications for exosomes: Are we there yet? *British Journal of Pharmacology*, *178*, 2375–2392.

Pužar Dominkuš, P., Stenovec, Mž, Sitar, S., Lasič, E., Zorec, R., Plemenitaš, A., Žagar, E., Kreft, M., & Lenassi, M. (2018). PKH26 labeling of extracellular vesicles: Characterization and cellular internalization of contaminating PKH26 nanoparticles. *Biochimica et Biophysica Acta Biomembranes*, *1860*, 1350–1361.

Samal, J., Rebelo, A. L., & Pandit, A. (2019). A window into the brain: Tools to assess pre-clinical efficacy of biomaterials-based therapies on central nervous system disorders. *Advanced Drug Delivery Reviews*, *148*, 68–145.

Saxena, S., Funk, M., & Chisholm, D. (2013). World health assembly adopts comprehensive mental health action plan 2013–2020. *Lancet*, *381*, 1970–1971.

Schulz-Siegmund, M., & Aigner, A. (2021). Nucleic acid delivery with extracellular vesicles. *Advanced Drug Delivery Reviews*, *173*, 89–111.

Shi, Y., Song, R., Wang, Z., Zhang, H., Zhu, J., Yue, Y., Zhao, Y., & Zhang, Z. (2021). Potential clinical value of circular RNAs as peripheral biomarkers for the diagnosis and treatment of major depressive disorder. *EBioMedicine*, *66*, 103337.

Shimomura, T., Seino, R., Umezaki, K., Shimoda, A., Ezoe, T., Ishiyama, M., & Akiyoshi, K. (2021). New lipophilic fluorescent dyes for labeling extracellular vesicles: Characterization and monitoring of cellular uptake. *Bioconjugate Chemistry*, *32*, 680–684.

Simonsen, J. B. (2019). Pitfalls associated with lipophilic fluorophore staining of extracellular vesicles for uptake studies. *Journal of Extracell Vesicles*, *8*, 1582237.

Smith, K. (2014). Mental health: A world of depression. *Nature*, *515*, 180.

Smyth, T., Kullberg, M., Malik, N., Smith-Jones, P., Graner, M. W., & Anchordoquy, T. J. (2015). Biodistribution and delivery efficiency of unmodified tumor-derived exosomes. *Journal of Controlled Release*, *199*, 145–155.

Song, A. -Q., Gao, B., Fan, J. -J., Zhu, Y. -J., Zhou, J., Wang, Y. -L., Xu, L. -Z., & Wu, W. -N. (2020). NLRP1 inflammasome contributes to chronic stress-induced depressive-like behaviours in mice. *Journal of Neuroinflammation*, *17*, 178.

Song, H., Li, X., Zhao, Z., Qian, J., Wang, Y., Cui, J., Weng, W., Cao, L., Chen, X., Hu, Y., & Su, J. (2019). Reversal of osteoporotic activity by endothelial cell-secreted bone targeting and biocompatible exosomes. *Nano Letters*, *19*, 3040–3048.

Song, R., Bai, Y., Li, X., Zhu, J., Zhang, H., Shi, Y., Li, K., Wang, Bi, Zhang, H., Yang, Y., & Zhang, Z. (2020). Plasma circular RNA DYM related to major depressive disorder and rapid antidepressant effect treated by visual cortical repetitive transcranial magnetic stimulation. *Journal of Affective Disorders*, *274*, 486–493.

Sutaria, D. S., Badawi, M., Phelps, M. A., & Schmittgen, T. D. (2017). Achieving the promise of therapeutic extracellular vesicles: The devil is in details of therapeutic loading. *Pharmaceutical Research*, *34*, 1053–1066.

Takov, K., Yellon, D. M., & Davidson, S. M. (2017). Confounding factors in vesicle uptake studies using fluorescent lipophilic membrane dyes. *Journal of Extracellular Vesicles*, *6*, 1388731.

Théry, C., Witwer, K. W., Aikawa, E., Alcaraz, M. J., Anderson, J. D., Andriantsitohaina, R., Antoniou, A., Arab, T., Archer, F., Atkin-Smith, G. K., Ayre, D. C., Bach, J. -M., Bachurski, D., Baharvand, H., Balaj, L., Baldacchino, S., Bauer, N. N., Baxter, A. A., Bebawy, M., …Zuba-Surma, E. K. (2018). Minimal information for studies of extracellular vesicles 2018 (MISEV2018): A position statement of the international society for extracellular vesicles and update of the MISEV2014 guidelines. *Journal of Extracellular Vesicles*, *7*, 1535750.

Thomson, D. W., & Dinger, M. E. (2016). Endogenous microRNA sponges: Evidence and controversy. *Nature Reviews Genetics*, *17*, 272–283.

Tian, Y., Li, S., Song, J., Ji, T., Zhu, M., Anderson, G. J., Wei, J., & Nie, G. (2014). A doxorubicin delivery platform using engineered natural membrane vesicle exosomes for targeted tumor therapy. *Biomaterials*, *35*, 2383–2390.

Trautner, T. A., Balganesh, T. S., & Pawlek, B. (1988). Chimeric multispecific DNA methyltransferases with novel combinations of target recognition. *Nucleic Acids Research*, *16*, 6649–6658.

Van Der Vlist, E. J., Nolte-'T Hoen, E. N. M., Stoorvogel, W., Arkesteijn, G. J. A., & Wauben, M. H. M. (2012). Fluorescent labeling of nano-sized vesicles released by cells and subsequent quantitative and qualitative analysis by high-resolution flow cytometry. *Nature Protocols*, *7*, 1311–1326.

Vu, L. T., Peng, B., Zhang, D. X., Ma, V., Mathey-Andrews, C. A., Lam, C. K., Kiomourtzis, T., Jin, J., Mcreynolds, L., Huang, L., Grimson, A., Cho, W. C., Lieberman, J., & Le, MTn (2019). Tumor-secreted extracellular vesicles promote the activation of cancer-associated fibroblasts via the transfer of microRNA-125b. *Journal of Extracellular Vesicles*, *8*, 1599680.

Wan, Z., Zhao, L., Lu, F., Gao, X., Dong, Y., Zhao, Y., Wei, M., Yang, G., Xing, C., & Liu, Li (2020). Mononuclear phagocyte system blockade improves therapeutic exosome delivery to the myocardium. *Theranostics*, *10*, 218–230.

Wang, J., Hodes, G. E., Zhang, H., Zhang, S., Zhao, W., Golden, S. A., Bi, W., Menard, C., Kana, V., Leboeuf, M., Xie, M., Bregman, D., Pfau, M. L., Flanigan, M. E., Esteban-Fernández, A., Yemul, S., Sharma, A., Ho, L., Dixon, R., …Pasinetti, G. M. (2018). Epigenetic modulation of inflammation and synaptic plasticity promotes resilience against stress in mice. *Nature Communication*, *9*, 477.

Wang, Y. -L., Han, Q. -Q., Gong, W. -Q., Pan, D. -H., Wang, L. -Z., Hu, W., Yang, M., Li, B., Yu, J., & Liu, Q. Microglial activation mediates chronic mild stress-induced depressive- and anxiety-like behaviour in adult rats. *Journal of Neuroinflammation*, *15*, 21.

Wiklander, O. P. B., Brennan, M. A., Lotvall, J., Breakefield, X. O., & El Andaloussi, S. (2019). Advances in therapeutic applications of extracellular vesicles. *Science Translational Medicine*, *11*, eaav8521.

Wiklander, O. P. B., Nordin, J. Z., O'loughlin, A., Gustafsson, Y., Corso, G., Mäger, I., Vader, P., Lee, Yi, Sork, H., Seow, Y., Heldring, N., Alvarez-Erviti, L., Smith, CiE, Le Blanc, K., Macchiarini, P., Jungebluth, P., Wood, M. J. A., & Andaloussi, S. (2015). Extracellular vesicle in vivo biodistribution is determined by cell source, route of administration and targeting. *Journal of Extracellular Vesicles*, *4*, 26316.

Willner, P. (1984). The validity of animal models of depression. *Psychopharmacology*, *83*, 1–16.

Wohleb, E. S., Terwilliger, R., Duman, C. H., & Duman, R. S. (2018). Stress-induced neuronal colony stimulating factor 1 provokes microglia-mediated neuronal remodeling and depressive-like behaviour. *Biological Psychiatry*, *83*, 38–49.

Wray, N. R., Ripke, S., Mattheisen, M., Trzaskowski, M., Byrne, E. M., Abdellaoui, A., Adams, M. J., Agerbo, E., Air, T. M., Andlauer, T. M. F., Bacanu, S. -A., Bækvad-Hansen, M., Beekman, A. F. T., Bigdeli, T. B., Binder, E. B., Blackwood, D. R. H., Bryois, J., Buttenschøn, H. N., Bybjerg-Grauholm, J., …Sullivan, P. F. (2018). Genome-wide association analyses identify 44 risk variants and refine the genetic architecture of major depression. *Nature Genetics*, *50*, 668–681.

Wu, H. -Y., Wu, J. -L., & Ni, Z. -L. (2019). Overexpression of microRNA-202-3p protects against myocardial ischemia-reperfusion injury through activation of TGF-beta1/Smads signaling pathway by targeting TRPM6. *Cell Cycle*, *18*, 621–637.

Wuensch, T., Thilo, F., Krueger, K., Scholze, A., Ristow, M., & Tepel, M. (2010). High glucose-induced oxidative stress increases transient receptor potential channel expression in human monocytes. *Diabetes*, *59*, 844–849.

Xu, Ye, Man, Na, Karl, D., Martinez, C., Liu, F., Sun, J., Martinez, C. J., Martin, G. M., Beckedorff, F., Lai, F., Yue, J., Roisman, A., Greenblatt, S., Duffort, S., Wang, L., Sun, X., Figueroa, M., Shiekhattar, R., & Nimer, S. (2019). TAF1 plays a critical role in AML1-ETO driven leukemogenesis. *Nature Communication*, *10*, 4925.

Yang, Y., Fan, X., Mao, M., Song, X., Wu, P., Zhang, Y., Jin, Y., Yang, Yi, Chen, L. -L., Wang, Y., Wong, CCl, Xiao, X., & Wang, Z. (2017). Extensive translation of circular RNAs driven by N(6)-methyladenosine. *Cell Research*, *27*, 626–641.

Yong, T., Zhang, X., Bie, N., Zhang, H., Zhang, X., Li, F., Hakeem, A., Hu, J., Gan, Lu, Santos, H. A., & Yang, X. (2019). Tumor exosome-based nanoparticles are efficient drug carriers for chemotherapy. *Nature Communication*, *10*, 3838.

Zhang, H., Chen, Z., Zhong, Z., Gong, W., & Li, J. (2018). Total saponins from the leaves of Panax notoginseng inhibit depression on mouse chronic unpredictable mild stress model by regulating circRNA expression. *Brain Behaviour*, *8*, e01127.

Zhang, Y., Du, L., Bai, Y., Han, B., He, C., Gong, L., Huang, R., Shen, L., Chao, J., Liu, P., Zhang, H., Zhang, H., Gu, L., Li, J., Hu, G., Xie, C., Zhang, Z., & Yao, H. (2020). CircDYM ameliorates depressive-like behaviour by targeting miR-9 to regulate microglial activation via HSP90 ubiquitination. *Molecular Psychiatry*, *25*, 1175–1190.

Zhang, Y., Huang, R., Cheng, M., Wang, L., Chao, J., Li, J., Zheng, P., Xie, P., Zhang, Z., & Yao, H. (2019). Gut microbiota from NLRP3-deficient mice ameliorates depressive-like behaviours by regulating astrocyte dysfunction via circHIPK2. *Microbiome*, *7*, 116.

SUPPORTING INFORMATION

Additional supporting information may be found in the online version of the article at the publisher's website.

How to cite this article: Yu, X., Bai, Y., Han, B., Ju, M., Tang, T., Shen, L., Li, M., Yang, Li, Zhang, Z., Hu, G., Chao, J., Zhang, Y., & Yao, H. (2022). Extracellular vesicle-mediated delivery of circDYM alleviates CUS-induced depressive-like behaviours. *Journal of Extracellular Vesicles*, *11*, e12185. https://doi.org/10.1002/jev2.12185